

GS-ROR²: Bidirectional-guided 3DGS and SDF for Reflective Object Relighting and Reconstruction

ZUO-LIANG ZHU, Nankai University, China
 BEIBEI WANG[†], Nanjing University, China
 JIAN YANG[†], Nankai University, China

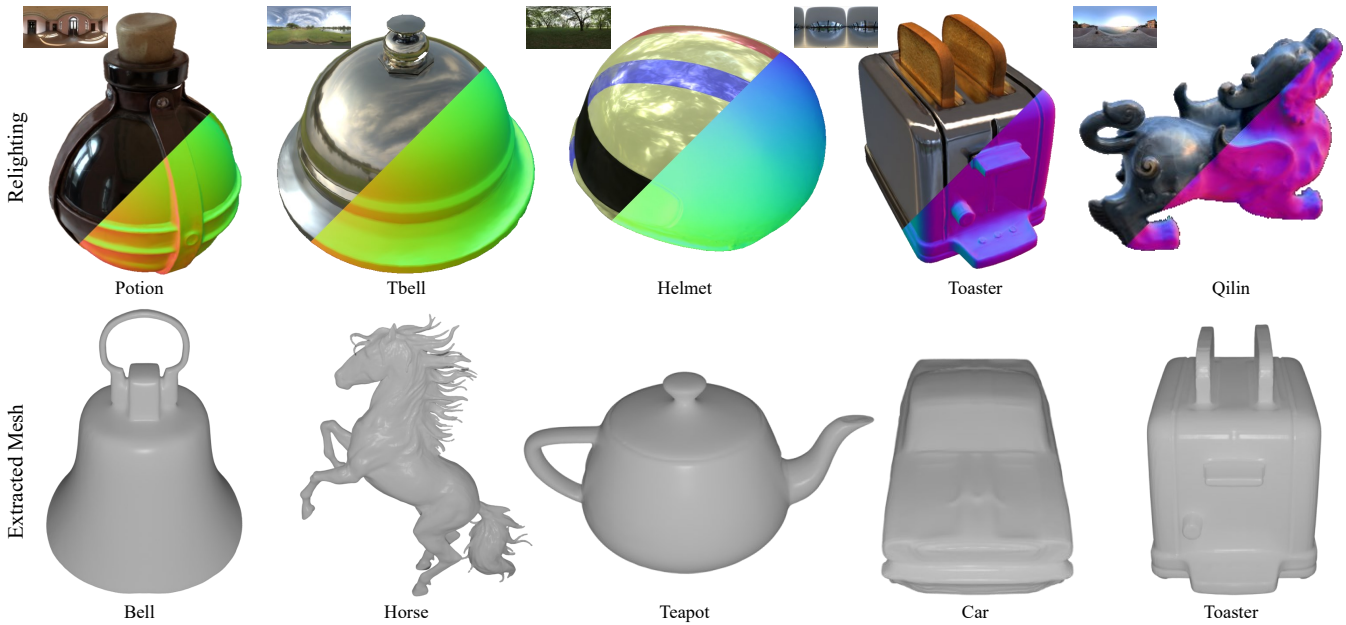


Fig. 1. We present bidirectional-guided 3DGS and SDF for **Reflective Object Relighting and Reconstruction** (GS-ROR²) from multi-view images. We show relighting results with reflective highlights (left) and their normal (right) in the 1st row, including POTION, TBELL from NeRO [Liu et al. 2023], HELMET, TOASTER from Ref-NeRF [Verbin et al. 2022], and QILIN from NeLLF++ [Zhang et al. 2023], where QILIN is a real scene. Besides, we show extracted meshes in the 2nd row, including BELL, HORSE, TEAPOT from NeRO and CAR, TOASTER from Ref-NeRF. Our method demonstrates a robust geometry reconstruction for reflective surfaces and faithful material decomposition, leading to photo-realistic reflective object relighting and high-fidelity geometry reconstruction.

3D Gaussian Splatting (3DGS) has shown a powerful capability for novel view synthesis due to its detailed expressive ability and highly efficient rendering speed. Unfortunately, creating relightable 3D assets and reconstructing faithful geometry with 3DGS is still problematic, particularly for reflective objects, as its discontinuous representation raises difficulties in constraining geometries. In contrary, volumetric signed distance field (SDF) methods provide robust geometry reconstruction, while the expensive ray marching hinders its real-time application and slows the training. Besides, these methods struggle to capture sharp geometric details. To this end, we propose to guide 3DGS and SDF bidirectionally in a complementary manner, including an SDF-aided Gaussian splatting for efficient optimization of the relighting model and a GS-guided SDF enhancement for high-quality geometry reconstruction. At the core of our SDF-aided Gaussian splatting is the *mutual supervision* of the depth and normal between blended Gaussians and SDF, which avoids the expensive volume rendering of SDF. Thanks to this mutual supervision, the learned blended Gaussians are well-constrained with

a minimal time cost. As the Gaussians are rendered in a deferred shading mode, the alpha-blended Gaussians are smooth, while individual Gaussians may still be outliers, yielding floater artifacts. Therefore, we introduce an SDF-aware pruning strategy to remove Gaussian outliers located distant from the surface defined by SDF, avoiding the floater issue. This way, our GS framework provides reasonable normal and achieves realistic relighting, while the mesh of truncated SDF (TSDF) fusion from depth is still problematic. Therefore, we design a GS-guided SDF refinement, which utilizes the blended normal from Gaussians to finetune SDF. Equipped with the efficient enhancement, our method can further provide high-quality meshes for reflective objects at the cost of 17% extra training time. Consequently, our method outperforms the existing Gaussian-based inverse rendering methods in terms of relighting and mesh quality. Our method also exhibits competitive relighting/mesh quality compared to NeRF-based methods with at most 25%/33% of training time and allows rendering at 200+ frames per second on an RTX4090. We will release the code.

[†] Corresponding author.

Authors' addresses: Zuo-Liang Zhu, Nankai University, China, nkuzhuzl@gmail.com; Beibei Wang[†], Nanjing University, China, beibei.wang@nju.edu.cn; Jian Yang[†], Nankai University, China, csjyang@nankai.edu.cn.

CCS Concepts: • **Computing methodologies** → **Rendering**.

Additional Key Words and Phrases: neural rendering, Gaussian splatting, relighting

1 INTRODUCTION

Creating relightable 3D assets from multi-view images has been a long-standing and challenging task in computer graphics and vision, as the decomposition of lighting, materials, and geometries is highly ill-posed. Particularly, the decomposition becomes more difficult for reflective objects, as their appearances are highly view-dependent, and a minor error on the surface leads to a significant difference. Existing approaches [Li et al. 2024; Liu et al. 2023] have shown impressive relighting quality for reflective objects by leveraging the neural radiance field (NeRF) and the signed distance field (SDF). Unfortunately, these methods require a long training and rendering time. They also struggle to capture sharp geometry details. In this paper, we aim at reflective object relighting and reconstruction given multi-view images, achieving high-quality relighting and detailed reconstruction with short training/rendering time costs.

Most recently, Kerbl et al. [2023] proposed 3D Gaussian Splatting (3DGS), boosting the rendering speed significantly and achieving more detailed appearance modeling. A concurrent work [Ye et al. 2024] has introduced deferred Gaussian splatting for reflective objects, improving the novel view synthesis (NVS) quality. Despite the impressive NVS quality, relighting and geometry reconstruction with 3DGS become problematic due to the Gaussians' discontinuity and high flexibility, especially for reflective objects. Extensive efforts have been made to improve the relighting quality by regularizing the geometry in terms of the normal and depth [Gao et al. 2024; Jiang et al. 2024; Liang et al. 2024]. However, they still suffer from erroneous surfaces and floater artifacts for reflective objects.

Some prior works (e.g., NeuSG [Chen et al. 2023], GSDF [Yu et al. 2024a]) couple SDF with GS for surface reconstruction. While their work has shown impressive reconstructed quality for diffuse objects, they require extensive training time and memory cost, due to the rendering of SDF and the existence of two representations. Our method focuses on both relighting and reconstruction, thus raising more difficulties. Specifically, evaluating the rendering equation increases the training time, and additional material parameters make the memory cost issue more obvious. These issues become more severe when modeling reflective objects, as the specular highlight is sensitive to the reflective direction, which needs more Gaussians to provide detailed normal. Therefore, introducing SDF into GS for our task is not straightforward, which raises the demand for a more efficient framework.

In this paper, we propose a bidirectional guidance of GS and SDF in a complementary manner, including an SDF-aided Gaussian splatting for efficient optimization of the relighting model and a GS-guided SDF enhancement for high-quality geometry reconstruction. Specifically, the SDF-aided Gaussian splatting utilizes the SDF to constrain the Gaussians with minimal computational increase. For this, we propose to supervise the deferred Gaussians and a low-resolution SDF mutually in our framework, so-called *mutual supervision*, which allows constraining deferred Gaussians with SDFs while avoiding SDF rendering. This way, the learned deferred Gaussians are better constrained. However, we still notice that Gaussians have floater artifacts occasionally, as the deferred Gaussians (with alpha blending) rather than individual Gaussians are constrained by SDF. Therefore, we introduce an SDF-aware pruning strategy

to remove Gaussian outliers to avoid this floater issue. Therefore, our method provides reasonable shading normal and enables realistic relighting for reflective objects in the GS framework. Due to the inconsistency between the normal and depth from blended Gaussians, the meshes of TSDF fusion from depth are still problematic. Meanwhile, SDF is underfitted and only learns the coarse structure of geometry. To solve this, we further design a GS-guided SDF enhancement, which utilizes the learned normal from fixed Gaussians to finetune the upsampled SDF. This way, we avoid optimizing a full-resolution SDF and GS jointly, reducing 40% of the memory requirement. SDF benefits from the detailed expressive ability of GS and learns more fine-grained geometry details. Equipped with this design, our method achieves high-quality geometry reconstruction for reflective objects from SDF with only 17% extra overhead of training time. Consequently, our method outperforms the existing Gaussian-based inverse rendering methods in terms of relighting and mesh quality. Meanwhile, it exhibits competitive relighting/mesh quality compared to NeRF-based methods with at most 25%/33% of training time. It also allows real-time rendering with 200+ frames per second on an RTX4090. To summarize, our main contributions include

- a GS-ROR² framework for reflective objects, achieving high-quality relighting and geometry reconstruction while maintaining short training time and allowing real-time rendering,
- an SDF-aided GS, including a mutual supervision between deferred Gaussians and the SDF with an SDF-aware Gaussian pruning strategy, producing robust geometry and avoiding local minima with minimal computational increase, and
- a GS-guided SDF enhancement via blended normal from Gaussians, enabling high-quality geometry reconstruction.

2 RELATED WORK

2.1 Neural representations for multi-view stereo

Since the presence of NeRF [Mildenhall et al. 2020], numerous neural implicit representations [Barron et al. 2022; Chen et al. 2022; Fridovich-Keil et al. 2022; Müller et al. 2022] have been proposed and gained remarkable progress in the field of multi-view stereo. These NeRF-based models adopt Multi-Layer Perceptrons (MLPs) [Barron et al. 2021, 2022; Verbin et al. 2022] or grid-like representations [Chen et al. 2022; Fridovich-Keil et al. 2022; Müller et al. 2022] to represent geometry and view-dependent appearance, optimized via volume rendering. Subsequently, NeuS [Wang et al. 2021] links the SDF with the density in NeRF and enables the optimization of surfaces with volume rendering. With extra regularization, these SDF-based models [Li et al. 2023; Rosu and Behnke 2023; Wang et al. 2023] achieve detailed surface reconstruction from RGB images. Owing to carefully designed architectures and specific optimization, some methods [Fridovich-Keil et al. 2022; Müller et al. 2022] enable fast training and real-time radiance field rendering.

3DGS [2023] sheds light on the multi-view stereo in the rasterization framework, providing impressive real-time NVS results. 3DGS utilizes the discrete explicit 3D Gaussian primitive and projects these primitives onto the image plane to obtain the pixel color via alpha blending, which avoids the consuming sampling operation.

However, 3DGS imposes no geometry constraint while optimizing, leading to noisy depth and normal, which hinders the usage of 3DGS in many downstream tasks. To resolve this issue, existing methods construct different constraints on Gaussians by introducing 2D Gaussian [Huang et al. 2024] or Gaussian Surfel [Dai et al. 2024]. SuGaR [Guédon and Lepetit 2024] extracts meshes from the Gaussians and binds the flattened Gaussians to the surface to optimize further. These new primitives and regularization could improve the geometry quality, potentially benefiting the relighting task.

Several previous works introduce SDF into 3DGS. NeuSG introduces SDF into 3DGS to improve the details of surface reconstruction by optimizing NeuS and 3DGS jointly. Despite the high quality of the reconstructed surface, the training time is tens of times longer than 3DGS. GSDF utilizes the depth from Gaussian to guide sampling for SDF, but they still need to render color in the SDF branch, leading to higher efficiency. While our method also incorporates the SDF and Gaussians, the key difference is that it drops SDF rendering, improving the geometry quality with a low time cost.

2.2 Inverse rendering

Inverse rendering aims to decompose geometry, material, and light from multi-view RGB images. Most existing methods adopt the geometry formulation from NeRF in either density or SDF manner, namely NeRF-based method. In terms of material modeling, most methods utilize the Disney Principled BRDF model [McAuley et al. 2013], while NeRFactor [Zhang et al. 2021b] pretrains a BRDF MLP with a measured BRDF dataset. Considering the light modeling, early works [Bi et al. 2020; Boss et al. 2021a,b; Zhang et al. 2022a, 2021a] consider direct light only, and recent works [Jin et al. 2023; Srinivasan et al. 2021; Sun et al. 2023; Yang et al. 2023; Zhang et al. 2023, 2022b] model indirect lighting and visibility, leading to a higher-quality decomposition. NeRF Emitter [Ling et al. 2024] incorporates NeRF as a non-distant emitter and uses importance sampling of NeRF to reduce rendering variance. Neural-PBIR [Sun et al. 2023] introduces the differentiable path tracing to model complex inter-reflection. However, these NeRF-based methods suffer from slow rendering speed and high memory usage in training.

More recently, Gaussian-based inverse rendering methods have begun to emerge. These methods regularize Gaussians to obtain better geometry in various ways. GShader [Jiang et al. 2024] and GIR [Shi et al. 2023] link the shortest axis of Gaussian with the normal. The GShader, R3DG [Gao et al. 2024], and GS-IR [Liang et al. 2024] supervise the Gaussian normal with the depth normal. To model the indirect illumination, R3DG, GIR, and GS-IR compute the visibility via one-step ray tracing and represent the indirect illumination with SH coefficients. These early Gaussian-based relighting methods cannot relight reflective objects, while our method enables such scenarios.

2.3 Reflective objects NVS and relighting

As a special and challenging case, NVS and relighting of reflective objects have drawn much attention. Ref-NeRF [Verbin et al. 2022] replaces the outgoing radiance with the incoming radiance and models the shading explicitly with an integrated direction encoding (IDE) to improve the quality of reflective materials. MS-NeRF [Yin et al. 2023]

designs a multi-space neural representation to model the reflection of mirror-like planes. Spec-NeRF [Ma et al. 2024] introduces a learnable Gaussian directional encoding to better model view-dependent effects. Spec-Gaussian [Yang et al. 2024] uses anisotropic spherical Gaussian to model view-dependent highlights. 3DGS-DR [Ye et al. 2024], as a concurrent work, introduces deferred shading into 3DGS. We also utilize a deferred framework, but for relighting, and together with other key components.

Another group of methods enables relighting for reflective materials. NeRO [Liu et al. 2023] proposes a novel light representation consisting of two MLPs for direct and indirect light, respectively. With explicit incorporation of the rendering equation, NeRO reconstructs reflective objects of high quality. Wang et al. [2024] represent the indirect light with a 5-dimensional function, so-called the 5D neural plenoptic function. Thanks to material-aware integral positional encoding, their method reduces the light sample per pixel during training and provides more accurate material decomposition. TensoSDF [Li et al. 2024] designs roughness-aware incorporation between the radiance and reflectance field for robust geometry reconstruction and proposes a novel tensorial representation with SDF, enabling fast SDF query. Although their representation is faster than the original SDF, it still needs hours of training time and cannot achieve real-time rendering. Recently some Gaussian-based methods enable reflective object relighting with the help of pretrained models. DeferredGS [Wu et al. 2024] utilizes the idea of deferred shading to improve the quality of the reflective-object relighting in the Gaussian framework. However, their method needs to distill reasonable geometry from a pretrained SDF, taking more than 3 hours on an RTX 4090 and thus losing the efficiency in training. GlossyGS [Lai et al. 2024] introduces the segmentation prior for a reasonable material estimation, while the segmentation model (i.e., DINOv2 [Oquab et al. 2024]) needs more than 3 days on 4 RTX A100 to finetune with custom data. Our method takes a further step in the reflective object relighting with 3D Gaussians and provides high-quality relighting results without any pretrained model, keeping highly efficient training and rendering. Furthermore, our method can provide high-quality mesh with efficient finetuning, while the existing Gaussian-based methods fail to provide high-quality meshes for reflective objects.

3 PRELIMINARIES AND MOTIVATION

In this section, we briefly review two ways for 3D scene representations and then discuss our motivation.

3D Gaussian Splatting. 3DGS represents a scene with a set of 3D Gaussians whose distribution is defined as

$$G(x) = e^{-\frac{1}{2}(x-\mu)^T \Sigma^{-1}(x-\mu)}, \quad (1)$$

where x is a position in the scene, μ is the mean of the Gaussian, and Σ denotes the covariance matrix of the 3D Gaussian, which is factorized into a scaling matrix S and a rotation matrix R as $\Sigma = RSS^T R^T$. To render an image, 3DGS projects the 3D Gaussians onto the image plane and employs alpha blending on the sorted 2D Gaussians as

$$C = \sum_{i=0}^n c_i \alpha_i \prod_{j=1}^{i-1} (1 - \alpha_j), \quad (2)$$

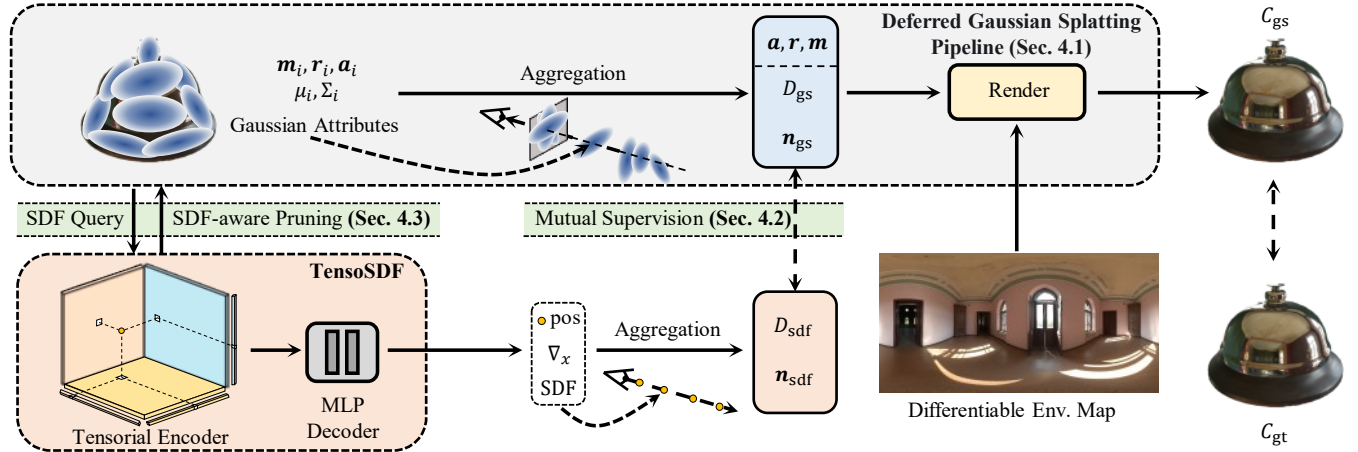


Fig. 2. Overview of our SDF-aided Gaussian Splatting. The architecture of our proposed method consists of two geometry representations (*i.e.*, Gaussian primitive and TensoSDF). In the deferred Gaussian pipeline, the shading parameters (*i.e.*, albedo \mathbf{a} , roughness \mathbf{r} and metallicity \mathbf{m}), normal and depth are projected to the image plane and alpha blended. The pixel color C_{gs} is calculated using the split-sum approximation and supervised by ground truth color C_{gt} . In the TensoSDF, we sample rays originated from camera center \mathbf{o} and view direction \mathbf{v} and query the SDF value and gradient for each point p along the ray $\mathbf{o} + t\mathbf{v}$. The normal \mathbf{n}_{sdf} and depth D_{sdf} are obtained via volume rendering, which is supervised mutually with the normal \mathbf{n}_{gs} the depth D_{gs} from Gaussians. Note no color network is used in the SDF part, and only the geometry attributes are volume rendered.

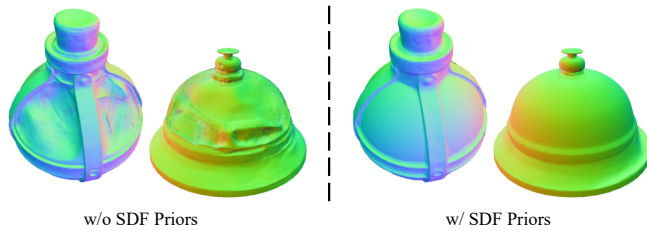


Fig. 3. The geometry from Gaussian is under-constrained and thus erroneous, while it is much better after utilizing the priors from the SDF.

where c_i is the color of each Gaussian, and α_i is given by evaluating a projected 2D Gaussian with covariance Σ' multiplied with a learned per-point opacity.

TensoSDF. An SDF expresses a scene by encoding the distance from the surface of an object, which can be expressed implicitly by an MLP [Wang et al. 2021] or in a hybrid way by combining explicit grids with a tiny MLP [Li et al. 2024], which allows more efficient training and rendering. Depth and normal are two significant attributes of geometry. In SDF, The point-wise depth D_i is defined as the distance from the camera to the sample, and the point-wise normal \mathbf{n}_i is the gradient of SDF ∇_x w.r.t. position x [Zhang et al. 2021a]. Given n points along the ray $p_i = \mathbf{o} + t\mathbf{v}$ where \mathbf{o} is the camera origin and \mathbf{v} is the view direction, we can aggregate these point-wise attributes to obtain the attributes (*i.e.*, depth, normal) of the hit point of the surface as:

$$D_{sdf} = \sum_{i=0}^n w_i D_i, \mathbf{n}_{sdf} = \sum_{i=0}^n w_i \mathbf{n}_i \quad (3)$$

where w_i is the weight of the i -th point derived from the SDF value.

SDF and NeRF can be unified by NeuS and VolSDF [Wang et al. 2021; Yariv et al. 2021], which maps an SDF value to a density distribution. The distribution in NeuS is defined as:

$$\phi_s(s) = \gamma e^{-\gamma s} / (1 + e^{-\gamma s})^2, \quad (4)$$

where s is the SDF value and γ is the inverse of standard deviation. Note that γ is a trainable parameter, and $1/\gamma$ approaches zero as the network training converges.

Among the SDF-based methods, TensoSDF utilizes a tensorial representation for SDF, consisting of a tensorial encoder and MLP decoder, which is formulated as follows:

$$V_p = v_k^X \circ M_k^{YZ} \oplus v_k^Y \circ M_k^{XZ} \oplus v_k^Z \circ M_k^{XY}, s = \Theta(V_p, p), \quad (5)$$

where v_k^m and $M_k^{\bar{m}}$ represent the k -th vector and matrix factors of their corresponding spatial axes m , and \bar{m} denotes the two axes orthogonal to m *e.g.*, $\bar{X} = YZ$. \circ and \oplus represent the element-wise multiplication and concatenation operations. V_p is the latent vector from the tensorial encoder and then is decoded with the position p by a tiny MLP Θ to get the SDF value s . The TensoSDF backbone enables faster convergence speed and low-cost SDF queries. Besides, the capacity of TensoSDF can be modulated efficiently through the interpolation of the tensorial grid.

Motivation. The above two representations can both express a 3D scene, where the Gaussian representation is explicit and discontinuous, and the SDF is implicit (or hybrid) and continuous. These two representations lead to different rendering methods: splatting or rasterization for Gaussians and sphere tracing for SDF. While the Gaussian representation significantly boosts the rendering speed to a real-time level, it has difficulties constraining geometries, leading to inferior geometries, as shown in Fig. 3. A straightforward idea is to incorporate these two representations by leveraging the SDF as a prior. However, rendering SDF is time-consuming, which hinders

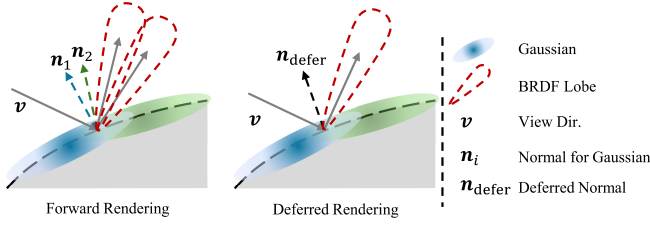


Fig. 4. Two Gaussians with a minor normal difference are overlapped to model an opaque surface. In the forward rendering, the BRDF values are computed w.r.t. to their own normal and are then alpha blended to form the final rendering, which is equivalent to a broader BRDF lobe, leading to a blurry rendering, eventually. In contrast, in the deferred shading, the BRDF is computed w.r.t. the deferred normal, maintaining the sharpness of reflective objects.

the benefits of 3DGS. Therefore, the essential problem is an elegant incorporation between the Gaussians and the SDF.

4 METHOD

This section presents our bidirectional-guided GS and SDF for reflective object relighting and reconstruction, named GS-ROR². First, we present an SDF-aided GS for relighting, including a deferred GS pipeline (Sec. 4.1), an SDF prior of mutual supervision for geometry regularization (Sec. 4.2), and an SDF-aware pruning to refine the Gaussian distribution (Sec. 4.3). Finally, we present a GS-guided SDF enhancement for high-quality geometry reconstruction (Sec. 4.4).

4.1 Deferred Gaussian splatting for relighting

Starting from GS-IR [Liang et al. 2024], we first construct a forward Gaussian splatting baseline for relighting, using the Disney Principled BDRF model [McAuley et al. 2013] and environment map to model the material and light. We drop the occlusion for efficiency and modify the normal formulation following Gaussian Shader [Jiang et al. 2024] as the combination of the shortest axis direction u and an offset n_δ as $\mathbf{n} = u + n_\delta$. The radiance from view \mathbf{v} for each Gaussian is computed by the split-sum approximation, following previous work [Jiang et al. 2024; Liang et al. 2024], and then aggregated by alpha blending. With multi-view images as inputs, the reflectance parameters at each Gaussian can be learned, besides the opacity and the environment map, enabling relighting under a novel environment map.

However, this simple Gaussian-based relighting baseline produces blurry relighting results for the reflective surface. The main reason behind this phenomenon is the alpha blending of Gaussians. As shown in Fig. 4, the Gaussians are overlapped to model an opaque surface with slightly different normals. While this difference among Gaussians causes a negligible error for rough objects, it amplifies the BRDF lobe for specular objects, leading to a blurry rendering. The key to addressing this issue is to blend the normals of Gaussians first and then perform shading, i.e., deferred shading.

Specifically, we perform alpha blending on all the attributes (e.g., normal, albedo, roughness) onto the image plane:

$$F = \sum_{i=0}^n f_i \alpha_i \prod_{j=1}^{i-1} (1 - \alpha_j), \quad (6)$$

where α_i, α_j share the same definition as in Eqn. (2), and f_i is a attribute of the i -th Gaussian. Then, we use split-sum approximation to compute the pixel-wise color.

The Gaussians are learned with the following loss function:

$$\mathcal{L}_{gs} = \mathcal{L}_c + \lambda_{nd} \mathcal{L}_{nd} + \lambda_{sm} \mathcal{L}_{sm} + \lambda_m \mathcal{L}_m + \lambda_{\delta n} \mathcal{L}_{\delta n}, \quad (7)$$

where \mathcal{L}_c is the color supervision between the rendered image and ground truth as in 3DGS, \mathcal{L}_{nd} is the supervision between the normal from Gaussian and from the estimated depth proposed in Gaussian Shader [Jiang et al. 2024], \mathcal{L}_{sm} is the smoothness loss for BRDF parameters, \mathcal{L}_m is the mask loss, and $\mathcal{L}_{\delta n}$ is the delta normal regularization in Gaussian Shader. More details are shown in Sec. 5.

4.2 An rendering-free mutual supervision

Thanks to the deferred Gaussian splatting, the blurry issue for reflective object relighting has been addressed. However, the geometry established by Gaussians exhibits erroneous surfaces and floaters, as it tends to overfit the appearance under training light conditions. Hence, more constraints on the geometry are needed. Inspired by NeRO and TensoSDF, we introduce SDF into our framework, as it has been shown to be a good prior for geometry regularization. The key is leveraging the capability of SDF while avoiding the expensive rendering. For this, we first choose a performance-friendly backbone for SDF – TensoSDF. Then, we propose geometry-only supervision between Gaussians and SDF, or so-called *mutual supervision*, together with the color supervision between Gaussians renderings and the input images, without any SDF rendering. On the one hand, as Gaussians build the link between rendered images and input images, they can supervise the training of SDF. On the other hand, the SDF can also constrain the Gaussians.

Mutual supervision. Even with a performance-friendly SDF backbone, TensoSDF rendering is still expensive, due to the complex color network required to faithfully represent the specular high-lights. Therefore, we propose to remove the SDF rendering and connect the SDF and Gaussians with geometry attributes.

Specifically, we pose supervision on the depth and normal of the SDF (Eqn. (3)) from Gaussians (Eqn. (2)):

$$\mathcal{L}_{gs2sdf} = |\mathbf{sg}[D_{gs}] - D_{sdf}| + (1 - \langle \mathbf{sg}[\mathbf{n}_{gs}], \mathbf{n}_{sdf} \rangle), \quad (8)$$

where D_{gs} and D_{sdf} are the depth from Gaussians and SDF, respectively, \mathbf{n}_{gs} and \mathbf{n}_{sdf} are normals from Gaussians and SDF respectively, and $\mathbf{sg}[\cdot]$ is the stop-gradient operation.

Besides the above loss, we also utilize the Eikonal loss \mathcal{L}_{eik} , Hessian loss \mathcal{L}_{hes} , mask loss \mathcal{L}_m , and total variance loss \mathcal{L}_{tv} to regularize the training of SDF, following common practice [Gropp et al. 2020; Li et al. 2024; Zhang et al. 2022c]. The final loss for SDF is

$$\mathcal{L}_{sdf} = \lambda_{gs2sdf} \mathcal{L}_{gs2sdf} + \lambda_{eik} \mathcal{L}_{eik} + \lambda_{hes} \mathcal{L}_{hes} + \lambda_m \mathcal{L}_m + \lambda_{tv} \mathcal{L}_{tv}. \quad (9)$$

where the $\lambda_{[\cdot]}$ is the corresponding coefficient to adjust the strength of regularization. Among these losses, our proposed \mathcal{L}_{gs2sdf} enables

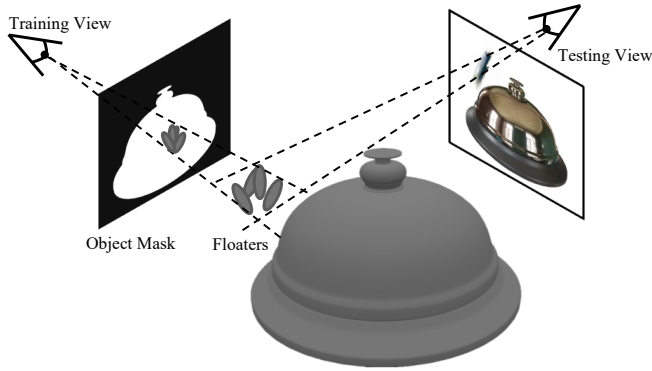


Fig. 5. In this example, the floaters can still be shown in the testing view, even if the mask loss was applied during training. The main reason is that although the floaters are shown outside the mask region in the testing view, they are within the mask region in the training views. Therefore, they can not be masked out by the mask loss.

the optimization of SDF via the geometry of Gaussians, and the \mathcal{L}_{eik} , \mathcal{L}_{hes} , \mathcal{L}_m , \mathcal{L}_{tv} regularize the SDF to obtain smooth and reasonable geometry.

Then, we design another loss to update Gaussians with SDF priors:

$$\mathcal{L}_{\text{sdf2gs}} = |D_{\text{gs}} - \mathbf{sg}[D_{\text{sdf}}]| + (1 - \langle \mathbf{n}_{\text{gs}}, \mathbf{sg}[\mathbf{n}_{\text{sdf}}] \rangle). \quad (10)$$

Finally, we obtain the mutual supervision $\mathcal{L}_{\text{gs2sdf}}$ and $\mathcal{L}_{\text{sdf2gs}}$, which bridges the SDF and Gaussian. Note that the stop-gradient operator is used to differ the strength of the supervisions of both sides.

Discussion. In general, SDF is optimized via color supervision between volume-rendered images and input images. However, our loss $\mathcal{L}_{\text{gs2sdf}}$ can optimize the SDF via depth and normal without color supervision, as the depth and the normal are derived from SDF, and thus the gradient from $\mathcal{L}_{\text{gs2sdf}}$ can optimize the SDF. In this way, we can drop the heavy color rendering and optimize the SDF with only geometry attributes (*i.e.*, depth and normal). With other widely used regularizations for SDF (*e.g.*, Eikonal loss), we can obtain a smooth and reasonable geometry from SDF. The loss $\mathcal{L}_{\text{sdf2gs}}$ regularizes the geometry of Gaussians in turn, so we can obtain a better decomposition between geometry and material from the Gaussians.

4.3 SDF-aware pruning

With the deferred Gaussians supervised by SDF priors, the geometry becomes smoother. However, we observe some artifacts caused by the overfitting on specular highlights of reflective objects in training views, which leads to Gaussian outliers distant from the surface. These overfitted Gaussians are in the mask region of all training views, so applying the mask loss cannot remove such outliers in training, and we still observe the floaters in the test view, as shown in Fig. 5. Besides, all the above losses supervise the alpha-blended results and lack constraints on individual Gaussians to handle the outliers. Therefore, we propose a Gaussian pruning strategy to enforce the Gaussians close to the zero-level set of SDF. Specifically, for each Gaussian, we check the SDF value at its center and discard

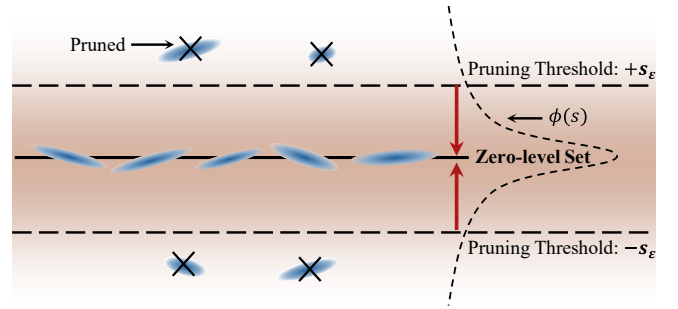


Fig. 6. The illustration of SDF-aware pruning. We define a narrowing threshold, which is adjusted automatically around the zero-level set. The Gaussians out of the threshold will be pruned. This pruning operation ensures all Gaussians are near the surface and avoids the floaters.

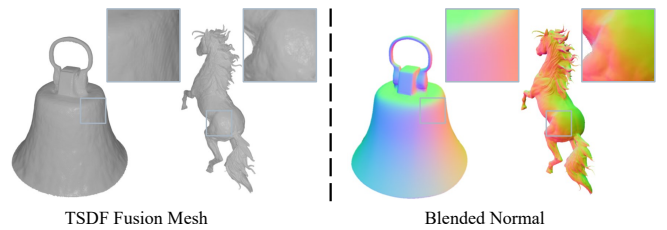


Fig. 7. Although the relighting framework ensures smooth blended normal to render realistic glossy highlight, the blended depth is inconsistent with the normal, and thus the mesh of TSDF fusion from depth can be problematic.

the Gaussian if the SDF value is larger than a threshold s_ϵ , as shown in the Fig. 6. Since it is laborious to adjust the threshold per scene, we link it with the probability density function $\phi_s(s)$ in Eqn. (4), and the threshold s_ϵ can be defined as $\phi_s(s_\epsilon) = p_t(s_\epsilon > 0)$ in the closed form:

$$s_\epsilon = \gamma \log(2p_t) - \gamma \log\left(\gamma^{-1} - 2p_t - \sqrt{\gamma^{-2} - 4p_t\gamma^{-1}}\right), \quad (11)$$

where p_t is an empirical hyperparameter and set to 0.01. In this way, the threshold is determined automatically and narrowed with the SDF in the optimization, so we avoid posing a constant too strict when the surface is under-reconstructed and prune the Gaussians too far away from the surface in the end.

4.4 GS-guided SDF enhancement

Due to the inconsistency between the normal and depth from blended Gaussians, as shown in Fig. 7, the meshes of TSDF fusion from depth can be problematic, even though the normal is well optimized in the GS framework. Lots of works [Chen et al. 2024; Moenne-Loccoz et al. 2024; Radl et al. 2024; Yu et al. 2024b] try to alleviate this inconsistency, while these solutions complicate the rendering pipeline and thus reduce the GS efficiency in training and rendering.

Since our framework has the TensoSDF as an extra geometry representation, we can directly extract mesh from it, without complicating the GS pipeline. Therefore, we propose the GS-guided SDF enhancement, which utilizes the normal from well-optimized

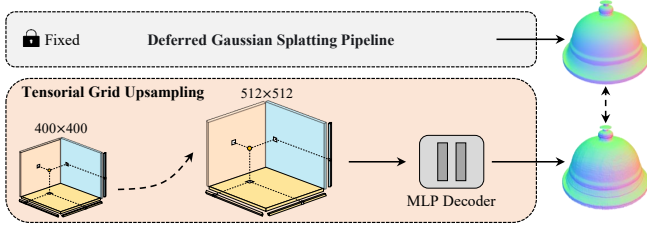


Fig. 8. The overview of GS-guided SDF enhancement. The TensoSDF learned from the first step is upsampled and refined by the blended normal from fixed Gaussians.

Gaussians to enable extracting high-quality meshes from TensoSDF.

Specifically, we first upsample the TensoSDF to capture the fine-grained details, which keeps a low resolution for efficiency in the first step. Then, the upsampled TensoSDF is finetuned efficiently via the learned normal from fixed Gaussians, as shown in Fig. 8. The loss for finetuning \mathcal{L}_{ft} is

$$\mathcal{L}_{ft} = (1 - \langle \mathbf{sg}[\mathbf{n}_{gs}], \mathbf{n}_{sdf} \rangle) + \lambda_{hes} \mathcal{L}_{hes} + \lambda_m \mathcal{L}_m + \lambda_{tv} \mathcal{L}_{tv}, \quad (12)$$

where all losses $\mathcal{L}_{[\cdot]}$ share the same definition as in Eqn. (9).

This way, the TensoSDF learns geometry details from the well-optimized Gaussians. Therefore, our method achieves high-quality geometry reconstruction for reflective objects, which beats the TensoSDF optimized via ray marching and uses only 33% training time of it. Compared to optimizing a full-resolution SDF and Gaussians jointly as in GSDF, we modulate the resolution of TensoSDF adaptively, leading to a more efficient framework and reducing the peak memory usage during optimization. Consequently, our framework maintains the highly efficient training/rendering from Gaussian splatting and meanwhile benefits from the robustness of the TensoSDF representation for geometry reconstruction.

5 IMPLEMENTATION DETAILS

This section presents the network structures and the training details.

Network structures. The TensoSDF has a resolution of 400×400 with feature channels set as 36, which upsamples to 512×512 further. The MLP decoder is a two-layer MLP whose width is 128. The Gaussian starts with 100K randomly initialized points.

Optimization details. The training of our framework includes three steps. Firstly, the deferred Gaussian splatting without SDF supervision is trained separately for 1K iterations with Eqn. (7) to obtain a coarse geometry. Then, we freeze the Gaussians and warm up the TensoSDF via the depth and normal from Gaussians Eqn. (9) for 3K iterations. Finally, we train the entire framework with a joint loss for 24K iterations:

$$\mathcal{L}_{joint} = \mathcal{L}_{gs} + \lambda_{sdf2gs} \mathcal{L}_{sdf2gs}. \quad (13)$$

We provide a table of loss functions (see Tab. 2) for better understanding and more details are in the supplementary material.

We train our model on an NVIDIA RTX 4090 and optimize it with Adam optimizer [Kingma and Ba 2017]. The learning rate for the TensoSDF [Li et al. 2024] grid and the MLP decoder is $1e^{-2}$

and $1e^{-3}$, respectively. The learning rate of Gaussian components follows the setting in 3DGS [Kerbl et al. 2023], and all attributes not in vanilla 3DGS have a learning rate of $2e^{-3}$. The initial resolution of TensoSDF is set to 128 and increases to the final resolution 400×400 , which uses only 60% capacity of the original TensoSDF, whose final resolution is 512×512 . The optimization procedure takes about 1.5 hours in total. After training, only Gaussians will be used for relighting. To extract high-quality meshes from TensoSDF, a 15-minute finetuning is needed, using the Adam optimizer and a cosine learning rate schedule. The learning rate for the TensoSDF [Li et al. 2024] grid and the MLP decoder starts with $1e^{-2}$ and $1e^{-3}$, which decays to $5e^{-4}$ and $5e^{-5}$ finally.

6 RESULTS

In this section, we describe the evaluation setup (Sec. 6.1), and evaluate our relighting and NVS results (Sec. 6.2). Then, we conduct ablation studies on several main components (Sec. 6.2) and discuss limitations (Sec. 6.4).

6.1 Evaluation setup

Dataset. We evaluate our method on three synthetic datasets and one real-scene dataset. We utilize the TensoIR [Jin et al. 2023] synthetic and Glossy Blender dataset [Liu et al. 2023] to evaluate the performance of diffuse and specular materials, respectively. Besides, we use the Shiny Blender dataset to show the generalization ability of our method for diverse materials. For real scenes, we select some specular objects from the NeRF++ [Zhang et al. 2023].

Methods for comparison. We select 7 representative methods for comparison. We choose MII [Zhang et al. 2022b], TensoIR [Jin et al. 2023], TensoSDF [Li et al. 2024], and NeRO [Liu et al. 2023] for NeRF-based methods and GShader [Jiang et al. 2024], GS-IR [Liang et al. 2024], and R3DG [Gao et al. 2024] for Gaussian-based methods. While evaluating the surface quality, we also select some non-relightable Gaussian-based reconstruction methods, including 2DGS, GOF [Yu et al. 2024b], and PGSR [Chen et al. 2024]. We trained these models based on their public codes and configurations. Note that we add the mask loss to train all the compared methods, for stabilizing training and fair comparison.

Metrics. We use the peak signal-to-noise ratio (PSNR) and structural similarity index (SSIM) [Wang et al. 2004] to measure the relighting quality of results for the comparison and ablation study in the main paper. We present the learned perceptual image patch similarity (LPIPS) [Zhang et al. 2018] in the supplementary materials. Due to the ambiguity between albedo and light, we normalize the relighting images to match the average colors of ground-truth images before computing the metrics, following NeRO. When the ground truth albedo is available, we rescale the relighting images based on the ground truth albedo and predicted albedo, following TensoIR. We use the mean angular error (MAE) and the Chamber distance (CD) to measure the quality of geometry reconstruction. We record the mean training time and the frame per second (FPS)¹

¹NeRO and TensoSDF use the Cycles Render Engine in Blender to provide relighting results, so the FPS depends on samples per pixel, which is 1024 following the NeRO setting.

Table 1. Relighting quality in terms of PSNR \uparrow and SSIM \uparrow on the Glossy Blender dataset. Numbers in **red** indicate the best performance, **orange** numbers indicate the second best, and numbers in **yellow** indicate the third best. Our method outperforms existing Gaussian-based methods. Note that although our quantitative metrics are lower than some NeRF-based methods, our training time is much shorter (25% of TensoSDF, 13% of NeRO).

	NeRF-based				Gaussian-based			
	MII	TensoIR	TensoSDF	NeRO	GShader	GS-IR	R3DG	Ours
	PSNR/SSIM	PSNR/SSIM	PSNR/SSIM	PSNR/SSIM	PSNR/SSIM	PSNR/SSIM	PSNR/SSIM	PSNR/SSIM
Angel	16.24/.8236	10.24/.2238	20.40/.8969	16.21/.7819	17.49/.8336	15.64/.6126	16.65/.8013	20.81/.8775
Bell	17.41/.8594	10.11/.1018	29.91/.9767	31.19/.9794	19.01/.8804	12.61/.2807	16.15/.8391	24.49/.9267
Cat	17.68/.8521	9.10/.1644	26.12/.9354	28.42/.9579	16.00/.8642	18.04/.7907	17.49/.8503	26.28/.9421
Horse	20.98/.8997	10.42/.1931	27.18/.9567	25.56/.9437	22.49/.9262	17.40/.7270	20.63/.8832	23.31/.9376
Luyu	17.89/.8050	8.27/.2375	19.91/.8825	26.22/.9092	15.62/.8254	19.00/.7727	17.47/.8168	22.61/.8995
Potion	17.13/.8094	6.21/.0846	27.71/.9422	30.14/.9561	12.33/.7575	16.37/.7051	14.99/.7799	25.67/.9175
Tbell	16.54/.8262	7.47/.1609	23.33/.9404	25.45/.9607	14.42/.8007	14.35/.5419	15.99/.7965	22.80/.9180
Teapot	16.71/.8546	9.96/.2093	25.16/.9482	29.87/.9755	18.21/.8560	16.63/.7646	17.36/.8389	21.17/.8932
Mean	17.57/.8413	8.97/.1719	24.97/.9349	26.63/.9331	16.95/.8430	16.26/.6494	17.09/.8258	23.39/.9140
Training Time	4h	5h	6h	12h	0.5h	0.5h	1h	1.5h
Ren. Time (FPS)	1/30	1/60	1/4	1/4	50	214	1.5	208

Table 2. Losses used in our paper.

Name	Apply on	Description
L_c	GS	Color supervision for 3DGS
L_{nd}	GS	Normal Consistency loss from GShader.
L_{sm}	GS	BRDF smoothness loss from R3DG.
$L_{\delta n}$	GS	Normal regularization for GShader.
L_{sdf2gs}	GS	The proposed depth/normal supervision for GS.
L_{gs2sdf}	SDF	The proposed depth/normal supervision for SDF.
L_{eik}	SDF	Eikonal loss from Gropp et al. [2020].
L_{hes}	SDF	Hessian Loss from Zhang et al. [2022c].
L_{tv}	SDF	Total variance loss from TensoRF.
L_m	GS/SDF	Mask loss for both 3DGS and SDF.

Table 3. Mesh quality in terms of CD \downarrow on the Glossy Blender dataset. (CD is multiplied by 10^2) Numbers in **red** indicate the best performance, and numbers in **orange** indicate the second best. Our method outperforms existing Gaussian-based methods.

	Non-relightable			Relightable			
	2DGS	GOF	PGSR	GShader	GS-IR	R3DG	Ours
Angel	0.93	0.73	0.54	0.85	1.77	0.98	0.41
Bell	3.35	3.07	1.65	1.10	11.53	4.18	0.31
Cat	2.74	2.25	2.93	2.56	5.88	3.39	1.34
Horse	1.18	1.07	0.73	0.73	1.96	1.35	0.34
Luyu	1.35	1.46	0.85	1.07	2.25	1.68	0.81
Potion	4.50	4.13	1.96	4.74	6.23	3.80	0.75
Tbell	5.50	4.61	4.72	5.74	10.21	5.00	0.55
Teapot	2.18	3.32	1.24	3.40	7.19	4.79	0.47
Mean	2.72	2.58	2.44	2.53	5.88	3.15	0.62

in the evaluation. All the FPS and training time are tested on an RTX 4090 unless otherwise specified.

6.2 Comparison with previous works

Relighting of reflective objects. We evaluate the relighting performance of specular materials on the Glossy Blender dataset. The quantitative measurements are shown in Tab. 1, and the relighting visualizations are placed in Fig. 14. Our method outperforms other Gaussian-based methods and achieves competitive results of the NeRF-based methods. We also show the decomposed maps in Fig. 15, Fig. 16, and Fig. 17. Due to the SDF priors and the deferred Gaussian splatting pipeline, our method can produce a smooth surface without losing details and predict reasonable BRDF parameters.

Relighting of diffuse objects. Although our design focuses on reflective surfaces, it can also show benefits for diffuse objects. We validate our method on the TensoIR dataset. The quantitative measurements are shown in Tab. 4. The comparison with NeRF-based methods and relighting visualizations are in the supplementary material. Our methods can outperform the existing Gaussian-based methods and some NeRF-based methods on the TensoIR dataset, which reveals the robustness under diverse materials.

Relighting on real data. For real scenes, we select some objects with specular highlights from NeILF++ [Zhang et al. 2023], and the results are shown in Fig. 18. As there is no available ground truth, we only show the reference training views and some results under novel light conditions. Our method produces reasonable relighting results under novel lighting. Besides, our method achieves a balance between quality and training speed, enabling reflective surface modeling with only 25% training time of TensoSDF and 13% of NeRO. Our method supports real-time rendering with 200+ FPS, much faster than all NeRF-based and some Gaussian-based methods.

NVS. We also present the NVS results on the Glossy Blender dataset and the Shiny Blender Dataset. The quantitative evaluation in terms of PSNR and SSIM is present in Tabs. 5 and 6. Our method

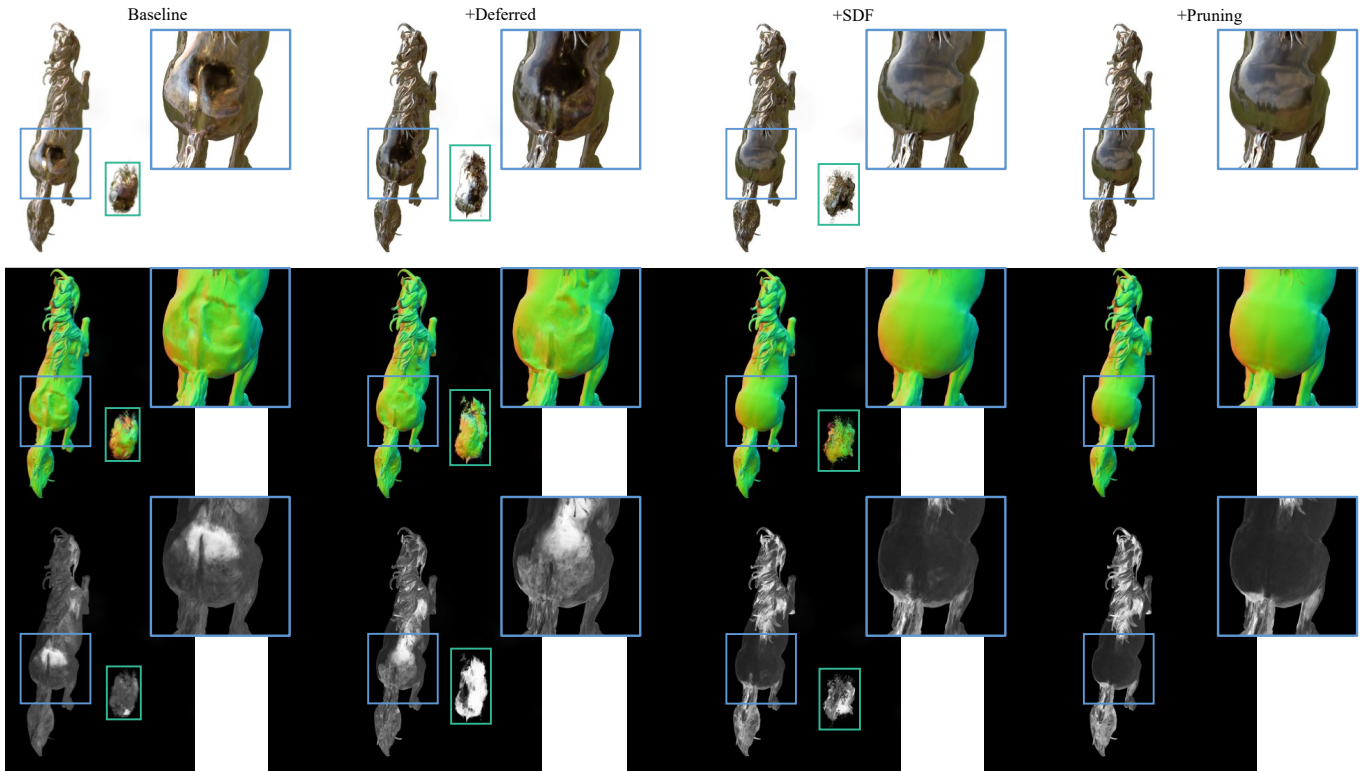


Fig. 9. Ablation of several key components in our method, including deferred shading, SDF supervision, and pruning. The first, second, and third rows show relighting results, normal, and roughness, respectively. The insets are shown in blue, and some floaters are shown in green.

Table 4. Relighting quality in terms of PSNR \uparrow and SSIM \uparrow on the TensorIR synthetic dataset. Numbers in **red** indicate the best performance, and numbers in **orange** indicate the second best.

	GShader	GS-IR	R3DG	Ours
	PSNR/SSIM	PSNR/SSIM	PSNR/SSIM	PSNR/SSIM
Armad.	22.86/.9280	27.65/.9078	30.76/.9526	31.33/.9593
Ficus	24.61/.9491	23.63/.8662	27.23/.9637	26.28/.9542
Hotdog	17.45/.8838	21.51/.8853	24.59/.9162	25.21/.9307
Lego	13.41/.7904	22.88/.8342	22.49/.8682	25.46/.9083
Mean	19.58/.8878	23.92/.8734	26.27/.9252	27.07/.9381

can provide high-quality NVS results with sharper highlights, which are present in Figs. 19 and 20, revealing the wide applications of our method. Our method outperforms the existing Gaussian-based methods on most scenes. However, our method fails in the Coffee scene, as the deferred pipeline assumes an opaque surface, and the liquid in the Coffee does not meet the assumption.

Geometry quality. We present the comparisons of geometry quality on the Shiny Blender and Glossy Blender datasets. The choice of measurement is based on the available ground truth. The normal estimation on the Shiny Blender dataset in Fig. 21 and MAE in Tab. 7. Thanks to the SDF priors, our method can provide robust normal

Table 5. NVS quality in terms of PSNR \uparrow and SSIM \uparrow on the Glossy Blender dataset. Numbers in **red** indicate the best performance, and numbers in **orange** indicate the second best.

	GS-IR	R3DG	GShader	Ours
	PSNR/SSIM	PSNR/SSIM	PSNR/SSIM	PSNR/SSIM
Angel	20.77/.6935	23.12/.7841	27.14/.9226	29.32/.9445
Bell	19.05/.4895	24.38/.8952	30.00/.9409	31.53/.9694
Cat	27.91/.9075	29.73/.9487	31.25/.9604	31.72/.9672
Horse	20.85/.6835	22.88/.7769	26.03/.9314	27.09/.9479
Luyu	24.96/.8637	25.97/.8986	27.35/.9175	28.53/.9383
Potion	25.81/.8217	29.03/.9277	29.53/.9357	30.51/.9503
Tbell	20.72/.6193	23.03/.8878	23.86/.9031	29.48/.9648
Teapot	20.56/.8427	20.82/.8719	23.56/.8986	26.41/.9468
Mean	22.58/.6322	24.87/.8739	27.34/.9263	29.32/.9537

estimation, while the results of other Gaussian-based methods are overfitted or noisy.

The CD on the Glossy Blender dataset is in Tab. 3. Our method achieves the best reconstruction quality regarding CD among the Gaussian-based methods. These Gaussian-based methods have no specific design for reflective objects, and some methods (e.g., PGSR) assume multi-view consistency of appearance, which does not hold

for reflective objects. Hence, all these methods perform poorly on the Glossy dataset. Although GSDF is most relevant to our method, it does not converge for reflective objects even with mask loss, and thus its result is not available. Besides, we show the mesh visualizations of representative methods in Fig. 22. Visually, the existing Gaussian-based methods cannot provide smooth surfaces. TensoSDF and NeRO can provide smooth meshes while discarding some geometry details (see the mane of ‘horse’). Our method can provide globally smooth meshes with geometry details.

6.3 Ablation study

We conduct ablation studies on the key components of our model on the Glossy Blender dataset. The mean relighting PSNR and SSIM are presented in the Tab. 10. We can see a consistent improvement when we employ new components to the model. We start from a baseline that first computes colors for Gaussians and alpha blends them as in 3DGS. As shown in the 1st column in Fig. 9, the baseline cannot render a reflective surface and provide the result with obvious artifacts due to the blending issue discussed in Sec. 4.1.

Deferred Gaussian splatting pipeline. After applying the deferred Gaussian splatting pipeline, this variant provides a more specular result. However, due to the erroneous normal, the surface reflects light from the wrong directions, shown in the 2nd column of Fig. 9. We observe more artifacts from the deferred results, for the pixel color from deferred shading corresponds to one shading point on the estimated surface while the one from forward shading is a

Table 6. NVS quality with Gaussian-based methods on Shiny Blender dataset in terms of PSNR \uparrow and SSIM \uparrow . Numbers in **red** indicate the best performance, and numbers in **orange** indicate the second best.

	GS-IR	R3DG	GShader	Ours
	PSNR/SSIM	PSNR/SSIM	PSNR/SSIM	PSNR/SSIM
Ball	18.30/.7584	21.39/.9047	30.40/.9623	35.50/.9849
Car	25.30/.8867	26.59/.9267	28.39/.9388	30.52/.9638
Coffee	30.72/.9463	32.57/.9710	30.79/.9690	29.64/.9568
Helmet	25.08/.9018	26.95/.9469	28.78/.9549	32.62/.9738
Teapot	38.21/.9900	43.86/.9963	43.35/.9957	43.88/.9964
Toaster	18.66/.7418	20.07/.8745	23.95/.9130	25.89/.9379
Mean	26.05/.8708	28.57/.9367	30.94/.9556	33.01/.9689

Table 7. Normal quality with Gaussian-based methods on Shiny Blender dataset in terms of MAE \downarrow . Numbers in **red** indicate the best performance, and numbers in **orange** indicate the second best.

	GS-IR	R3DG	GShader	Ours
Ball	25.79	22.44	7.03	0.92
Car	28.31	26.02	14.05	11.98
Coffee	15.38	13.39	14.93	12.24
Helmet	25.58	19.63	9.33	4.10
Teapot	15.35	9.21	7.17	5.88
Toaster	33.51	28.17	13.08	8.24
Mean	23.99	19.81	10.93	7.23



Fig. 10. Our method preserves the details that are lost in the SDF-based method (i.e., NeRO), revealing the benefits of the Gaussian representation.

Table 8. Comparison of the relighting quality between mutual supervision (Ours), using a pretrained TensoSDF to supervise Gaussians unidirectionally (Pretrained), and jointly optimization of full-resolution SDF with GS (Joint opt.) as in GSDF on the Glossy Blender dataset. Despite the slight improvement, using the pretrained model leads to an extensive training time or memory cost.

	Angel	Cat	Horse
Ours	20.81	26.28	23.31
Pretrained	21.45 (+0.64/+5h)	26.37 (+0.09/+5h)	24.59 (+1.28/+5h)
Joint opt.	21.68 (+0.87/+8.5GB)	26.50 (+0.22/+8.5GB)	24.34 (+1.03/+8.5GB)

combination of rendered colors of multiple Gaussians. The deferred formulation leaves less freedom for individual Gaussians to overfit. Consequently, more Gaussian outliers are generated to overfit sharp highlights, causing additional artifacts. Nevertheless, the deferred shading is necessary for specular materials (Sec. 4.1), and its issue has been solved in our full model.

TensoSDF incorporation. Then, we incorporate the TensoSDF and utilize its priors to regularize the geometry. The model without TensoSDF is vulnerable to local minima and overfits under the training light condition, leading to erroneous geometry estimation. After employing the TensoSDF (3rd column in Fig. 9), the model mitigates the ambiguity between material and geometry, thus predicting reasonable normal and material parameters (e.g., roughness). We validate the effectiveness of our mutual supervision by comparing it to supervision by a pretrained TensoSDF. As shown in Tab. 8, although using the pretrained TensoSDF for supervision could improve the quality slightly, it needs 5 hours for TensoSDF training. Optimizing GS with full-resolution SDF, as in GSDF, also improves the performance, increasing 40% (+8.5GB) memory usage. In contrast, our method achieves a balance between performance and efficiency. Besides, our method preserves the details while SDF-based methods fail, as shown in Fig. 10 (see the cat whisker), revealing the benefits of our Gaussian representation.

SDF-aware pruning. Eventually, we apply the SDF-aware pruning operation to our model. The models without pruning are likely to overfit under training views, and we can observe some unnecessary Gaussians under test views, causing severe floaters. Note that the overfitted Gaussians are invisible and in the mask region in training views. Therefore, we still observe the floater in the testing views, even though we apply the mask loss during training. After applying pruning, all Gaussians are located near the surface at the end of the

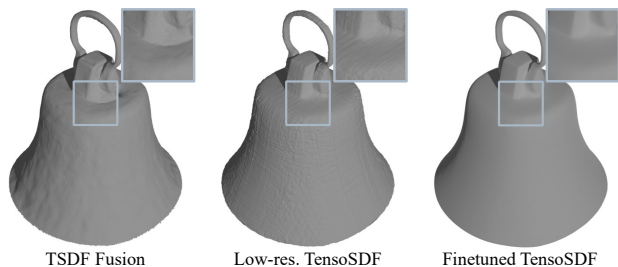


Fig. 11. The reconstruction results from TSDF fusion, low-res. TensoSDF and finetuned TensoSDF. The meshes from TSDF fusion and low-res. TensoSDF has obvious artifacts, while our finetuned TensoSDF provides globally smooth meshes with fine-grained details.

Table 9. Comparison of the mesh quality regarding CD \downarrow . (CD is multiplied by 10^2) We compare three variants: the mesh of TSDF fusion from Gaussians, the mesh from low-resolution TensoSDF, and our finetuned TensoSDF.

	Angel	Cat	Horse
TSDF Fusion	0.63	2.22	0.61
Low-res. TensoSDF	0.61	1.35	0.44
finetuned TensoSDF	0.41	1.34	0.34

Table 10. Ablation study of three key components on the Glossy Blender dataset. “Def.” means the deferred Gaussian splatting pipeline, “Inc.” means the incorporation of SDF and Gaussian, and “Pru.” means the pruning operation.

Components			Scene		
Def.	Inc.	Pru.	Angel	Cat	Horse
			PSNR/SSIM	PSNR/SSIM	PSNR/SSIM
			18.86/0.8562	24.18/0.9253	20.33/0.9012
✓			18.86/0.8574	24.87/0.9323	20.59/0.9089
✓	✓		20.48/0.8793	26.22/0.9417	23.12/0.9357
✓	✓	✓	20.81/0.8775	26.28/0.9421	23.31/0.9376

training, and the model provides relighting results without floater, as shown in the 4th column in Fig. 9.

GS-guided TensoSDF enhancement. The above designs ensure a promising normal for relighting, while the enhancement enables high-quality geometry reconstruction. We show the visualization of meshes from TSDF fusion, low-resolution TensoSDF, and finetuned TensoSDF in Fig. 11. Due to the inconsistency between the normal and depth of Gaussian primitives, though the blended normal is smooth, the artifacts are apparent in the mesh from TSDF fusion. Furthermore, the low-resolution TensoSDF cannot provide smooth meshes and leads to grid-like artifacts. After finetuning, the upsampled TensoSDF provides globally smooth meshes with fine-grained details. We also measure the mesh quality regarding CD in Tab. 9, and our finetuned TensoSDF provides the best performance. Note that we do not present the results of optimizing full-resolution TensoSDF with Gaussians, since this variant always leads to out-of-memory on the Glossy dataset.



Fig. 12. The comparison between the result using Cycle path-tracing renderer in Blender and the one using split-sum approximation in DiffRast. The split-sum result is blurry with extremely low roughness.

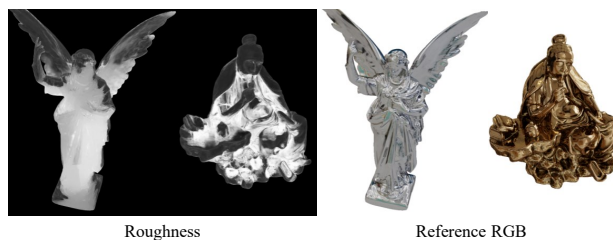


Fig. 13. Due to the lack of indirect illumination modeling, our method fails to decompose reasonable material parameters (e.g., roughness) on the concave surface with complex inter-reflection.

6.4 Discussion and limitations

In this part, we discuss several key differences between our method and other SDF-based methods. We mainly discuss two groups of closely related methods. The first group is the ones that optimize GS and SDF jointly (e.g., NeuSG, GSDF), and the second is the volumetric SDF methods. Then, we demonstrate some limitations of our methods and their potential solutions.

GS with SDF. Existing methods that optimize GS with SDF are designed for surface reconstruction and model the appearance by radiance, thus not supporting relighting. Due to the simplified appearance model, these methods fail to reconstruct reflective objects. NeuSG links SDF with GS only by aligning their normal. SDF and GS benefit marginally from each other, so it still takes 16 hours on an RTX 4090 for training. GSDF accelerates ray sampling of SDF by Gaussian depth and controls Gaussian opacity by SDF value. However, their method optimizes a full-resolution SDF with GS, which still takes 2 hours on an RTX A100 for training and encounters out-of-memory (OOM) issues. On the contrary, we utilize a low-resolution TensoSDF to regularize GS with mutual supervision, which is more efficient and avoids OOM. Additionally, we use the normal from fixed GS to enhance the geometry details of full-resolution TensoSDF efficiently. Note that though DeferredGS introduces SDF into GS, it only uses the pretrained SDF to regularize GS, while SDF cannot benefit from GS.

Volumetric SDF. Another group is the volumetric SDF-based methods that support relighting. As discussed in related works, these methods take a long time to converge, especially for the ones that handle reflective objects. We compare the open-source methods in the experiment section, while Neural-PBIR does not release the code. Its idea of introducing the differentiable path tracing to model complex inter-reflection could benefit the Gaussian-based methods.

Limitations. Our model improves the relighting and mesh quality compared to other Gaussian-based methods. However, some issues remain to be solved. We observe the split-sum approximation in DiffRast [Laine et al. 2020] causes blurry renderings for low-roughness surfaces. We render a mirror-like plane using the Cycle path-tracing renderer in Blender and the split-sum approximation in the DiffRast. The comparison is in Fig. 12, and the split-sum result is blurry. We believe replacing it with more accurate rendering methods will improve the relighting quality. Last, we only consider direct lighting in our framework, which causes inconsistent material decomposition in the regions with complex inter-reflection, as shown in Fig. 13. Introducing indirect illumination will benefit the relighting quality. We leave it for future work.

7 CONCLUSION

In this paper, we present a novel framework for real-time reflective object inverse rendering. We design an SDF-aided Gaussian splatting framework, using the mutual supervision of the depth and normal between deferred Gaussians and SDF to improve the geometry quality from Gaussians. Besides, we propose an SDF-aware pruning strategy with an automatically adjusted threshold, regularizing the position of Gaussian and avoiding the floater artifact. Finally, we design a GS-guided SDF enhancement to extract high-quality mesh by finetuning the TensoSDF. Consequently, our method outperforms the existing Gaussian-based inverse rendering methods without losing efficiency. It is competitive with the NeRF-based methods in terms of relighting and mesh quality, with much less training and rendering time. In future work, extending our framework to complex scenarios with multiple objects is a potential direction.

REFERENCES

- Jonathan T. Barron, Ben Mildenhall, Matthew Tancik, Peter Hedman, Ricardo Martin-Brualla, and Pratul P. Srinivasan. 2021. Mip-NeRF: A Multiscale Representation for Anti-Aliasing Neural Radiance Fields. In *ICCV*. IEEE, New York, NY, USA, 5855–5864.
- Jonathan T. Barron, Ben Mildenhall, Dor Verbin, Pratul P. Srinivasan, and Peter Hedman. 2022. Mip-NeRF 360: Unbounded Anti-Aliased Neural Radiance Fields. In *CVPR*. IEEE, New York, NY, USA, 5470–5479.
- Sai Bi, Zexiang Xu, Pratul Srinivasan, Ben Mildenhall, Kalyan Sunkavalli, Miloš Hašan, Yannick Hold-Geoffroy, David Kriegman, and Ravi Ramamoorthi. 2020. Neural Reflectance Fields for Appearance Acquisition. arXiv:2008.03824
- Mark Boss, Raphael Braun, Varun Jampani, Jonathan T. Barron, Ce Liu, and Hendrik P.A. Lensch. 2021a. NeRD: Neural Reflectance Decomposition From Image Collections. In *ICCV*. IEEE, New York, NY, USA, 12684–12694.
- Mark Boss, Varun Jampani, Raphael Braun, Ce Liu, Jonathan Barron, and Hendrik P.A. Lensch. 2021b. Neural-PIL: Neural Pre-Integrated Lighting for Reflectance Decomposition. In *NeurIPS*, M. Ranzato, A. Beygelzimer, Y. Dauphin, P.S. Liang, and J. Wortman Vaughan (Eds.), Vol. 34. Curran Associates, Inc., Red Hook, NY, USA, 10691–10704.
- Anpei Chen, Zexiang Xu, Andreas Geiger, Jingyi Yu, and Hao Su. 2022. TensorRF: Tensorial Radiance Fields. In *ECCV*. Springer, Berlin, Heidelberg, 333–350. https://doi.org/10.1007/978-3-031-19824-3_20
- Danpeng Chen, Hai Li, Weicai Ye, Yifan Wang, Weijian Xie, Shangjin Zhai, Nan Wang, Haomin Liu, Hujun Bao, and Guofeng Zhang. 2024. PGSR: Planar-based gaussian splatting for efficient and high-fidelity surface reconstruction. *IEEE TVCG* (2024).
- Hanlin Chen, Chen Li, and Gim Hee Lee. 2023. NeuSG: Neural Implicit Surface Reconstruction with 3D Gaussian Splatting Guidance. arXiv:2312.00846
- Pinxuan Dai, Jiamin Xu, Wenxiang Xie, Xinguo Liu, Huamin Wang, and Weiwei Xu. 2024. High-quality Surface Reconstruction using Gaussian Surfels. In *SIGGRAPH (SIGGRAPH '24)*. Association for Computing Machinery, New York, NY, USA, Article 22, 11 pages. <https://doi.org/10.1145/3641519.3657441>
- Sara Fridovich-Keil, Alex Yu, Matthew Tancik, Qinhong Chen, Benjamin Recht, and Angjoo Kanazawa. 2022. Plenoxels: Radiance Fields Without Neural Networks. In *CVPR*. IEEE, New York, NY, USA, 5501–5510.
- Jian Gao, Chun Gu, Youtian Lin, Zhihao Li, Hao Zhu, Xun Cao, Li Zhang, and Yao Yao. 2024. Relightable 3D Gaussians: Realistic Point Cloud Relighting with BRDF Decomposition and Ray Tracing. arXiv:2311.16043
- Amos Gropp, Lior Yariv, Niv Haim, Matan Atzmon, and Yaron Lipman. 2020. Implicit geometric regularization for learning shapes. In *ICML (ICML '20)*. JMLR.org, Article 355, 11 pages.
- Antoine Guédon and Vincent Lepetit. 2024. SuGaR: Surface-Aligned Gaussian Splatting for Efficient 3D Mesh Reconstruction and High-Quality Mesh Rendering. In *CVPR*. IEEE, New York, NY, USA, 5354–5363.
- Binbin Huang, Zehao Yu, Anpei Chen, Andreas Geiger, and Shenghua Gao. 2024. 2D Gaussian Splatting for Geometrically Accurate Radiance Fields. In *SIGGRAPH (SIGGRAPH '24)*. Association for Computing Machinery, New York, NY, USA, Article 32, 11 pages. <https://doi.org/10.1145/3641519.3657428>
- Yingwenqi Jiang, Jiadong Tu, Yuan Liu, Xifeng Gao, Xiaoxiao Long, Wenping Wang, and Yueshin Ma. 2024. GaussianShader: 3D Gaussian Splatting with Shading Functions for Reflective Surfaces. In *CVPR*. IEEE, New York, NY, USA, 5322–5332.
- Haian Jin, Isabella Liu, Peijia Xu, Xiaoshuai Zhang, Songfang Han, Sai Bi, Xiaowei Zhou, Zexiang Xu, and Hao Su. 2023. TensorIR: Tensorial Inverse Rendering. In *CVPR*. IEEE, New York, NY, USA, 165–174.
- Bernhard Kerbl, Georgios Kopanas, Thomas Leimkühler, and George Drettakis. 2023. 3D Gaussian Splatting for Real-Time Radiance Field Rendering. *ACM TOG* 42, 4 (2023), 139–1.
- Diederik P. Kingma and Jimmy Ba. 2017. Adam: A Method for Stochastic Optimization. arXiv:1412.6980
- Shuichang Lai, Letian Huang, Jie Guo, Kai Cheng, Bowen Pan, Xiaoxiao Long, Jiangjing Lyu, Chengfei Lv, and Yanwen Guo. 2024. GlossyGS: Inverse Rendering of Glossy Objects with 3D Gaussian Splatting. arXiv:2410.13349
- Samuli Laine, Janne Hellsten, Tero Karras, Yeongho Seol, Jaakko Lehtinen, and Timo Aila. 2020. Modular primitives for high-performance differentiable rendering. *ACM TOG* 39, 6, Article 194 (November 2020), 14 pages. <https://doi.org/10.1145/3414685.3417861>
- Jia Li, Lu Wang, Lei Zhang, and Beibei Wang. 2024. TensoSDF: Roughness-aware Tensorial Representation for Robust Geometry and Material Reconstruction. *ACM TOG* 43, 4, Article 150 (July 2024), 13 pages. <https://doi.org/10.1145/3658211>
- Zhaoshuo Li, Thomas Müller, Alex Evans, Russell H. Taylor, Mathias Unberath, Ming-Yu Liu, and Chen-Hsuan Lin. 2023. Neuralangelo: High-Fidelity Neural Surface Reconstruction. In *CVPR*. IEEE, New York, NY, USA, 8456–8465.
- Zhihao Liang, Qi Zhang, Ying Feng, Ying Shan, and Kui Jia. 2024. GS-IR: 3D Gaussian Splatting for Inverse Rendering. In *CVPR*. IEEE, New York, NY, USA, 21644–21653.
- Jingwang Ling, Ruihan Yu, Feng Xu, Chun Du, and Shuang Zhao. 2024. NeRF as a Non-Distant Environment Emitter in Physics-based Inverse Rendering. In *SIGGRAPH (SIGGRAPH '24)*. Association for Computing Machinery, Denver, CO, USA, Article 39, 12 pages. <https://doi.org/10.1145/3641519.3657404>

- Yuan Liu, Peng Wang, Cheng Lin, Xiaoxiao Long, Jiepeng Wang, Lingjie Liu, Taku Komura, and Wenping Wang. 2023. NeRO: Neural Geometry and BRDF Reconstruction of Reflective Objects from Multiview Images. *ACM TOG* 42, 4, Article 114 (July 2023), 22 pages. <https://doi.org/10.1145/3592134>
- Li Ma, Vasu Agrawal, Haithem Turki, Changil Kim, Chen Gao, Pedro Sander, Michael Zollhöfer, and Christian Richardt. 2024. SpecNeRF: Gaussian Directional Encoding for Specular Reflections. arXiv:2312.13102
- Stephen McAuley, Stephen Hill, Adam Martinez, Ryusuke Villemin, Matt Pettineo, Dimitar Lazarov, David Neubelt, Brian Karis, Christophe Hery, Naty Hoffman, and Hakan Zap Andersson. 2013. Physically based shading in theory and practice. In *ACM SIGGRAPH 2013 Courses (SIGGRAPH '13)*. Association for Computing Machinery, New York, NY, USA, Article 22, 8 pages. <https://doi.org/10.1145/2504435.2504457>
- Ben Mildenhall, Pratul P. Srinivasan, Matthew Tancik, Jonathan T. Barron, Ravi Ramamoorthi, and Ren Ng. 2020. NeRF: Representing Scenes as Neural Radiance Fields for View Synthesis. In *ECCV*. Springer, Berlin, Heidelberg, 405–421.
- Nicolas Moenne-Loccoz, Ashkan Mirzaei, Or Perel, Riccardo de Lutio, Janick Martinez Esturo, Gavriel State, Sanja Fidler, Nicholas Sharp, and Zan Gojic. 2024. 3D Gaussian Ray Tracing: Fast Tracing of Particle Scenes. *ACM Transactions on Graphics and SIGGRAPH Asia* (2024).
- Thomas Müller, Alex Evans, Christoph Schied, and Alexander Keller. 2022. Instant neural graphics primitives with a multiresolution hash encoding. *ACM TOG* 41, 4, Article 102 (July 2022), 15 pages. <https://doi.org/10.1145/3528223.3530127>
- Maxime Oquab, Timothée Darcet, Théo Moutakanni, Huy Vo, Marc Szafraniec, Vasil Khalidov, Pierre Fernandez, Daniel Haziza, Francisco Massa, Alaaeldin El-Nouby, Mahmoud Assran, Nicolas Ballas, Wojciech Galuba, Russell Howes, Po-Yao Huang, Shang-Wen Li, Ishan Misra, Michael Rabbat, Vasu Sharma, Gabriel Synnaeve, Hu Xu, Hervé Jegou, Julien Mairal, Patrick Labatut, Armand Joulin, and Piotr Bojanowski. 2024. DINOv2: Learning Robust Visual Features without Supervision. arXiv:2304.07193
- Lukas Radl, Michael Steiner, Mathias Parger, Alexander Weinrauch, Bernhard Kerbl, and Markus Steinberger. 2024. StopThePop: Sorted Gaussian Splatting for View-Consistent Real-time Rendering. *ACM Trans. Graph.* 43, 4, Article 64 (July 2024), 17 pages. <https://doi.org/10.1145/3658187>
- Radu Alexandru Rosu and Sven Behnke. 2023. PermutoSDF: Fast Multi-View Reconstruction With Implicit Surfaces Using Permutohedral Lattices. In *CVPR*. IEEE, New York, NY, USA, 8466–8475.
- Yahao Shi, Yanmin Wu, Chenming Wu, Xing Liu, Chen Zhao, Haocheng Feng, Jingtuo Liu, Liangjun Zhang, Jian Zhang, Bin Zhou, Errui Ding, and Jingdong Wang. 2023. GIR: 3D Gaussian Inverse Rendering for Relightable Scene Factorization. arXiv:2312.05133
- Pratul P. Srinivasan, Boyang Deng, Xiuming Zhang, Matthew Tancik, Ben Mildenhall, and Jonathan T. Barron. 2021. NeRV: Neural Reflectance and Visibility Fields for Relighting and View Synthesis. In *CVPR*. IEEE, New York, NY, USA, 7495–7504.
- Cheng Sun, Guangyan Cai, Zhengqin Li, Kai Yan, Cheng Zhang, Carl Marshall, Jia-Bin Huang, Shuang Zhao, and Zhao Dong. 2023. Neural-PBIR Reconstruction of Shape, Material, and Illumination. In *ICCV*. IEEE, New York, NY, USA, 18046–18056.
- Dor Verbin, Peter Hedman, Ben Mildenhall, Todd Zickler, Jonathan T. Barron, and Pratul P. Srinivasan. 2022. Ref-NeRF: Structured View-Dependent Appearance for Neural Radiance Fields. In *CVPR*. IEEE, New York, NY, USA, 5491–5500.
- Haoyuan Wang, Wenbo Hu, Lei Zhu, and Rynson W.H. Lau. 2024. Inverse Rendering of Glossy Objects via the Neural Plenoptic Function and Radiance Fields. In *CVPR*. IEEE, New York, NY, USA, 19999–20008.
- Peng Wang, Lingjie Liu, Yuan Liu, Christian Theobalt, Taku Komura, and Wenping Wang. 2021. NeuS: Learning Neural Implicit Surfaces by Volume Rendering for Multi-view Reconstruction. In *NeurIPS*, M. Ranzato, A. Beygelzimer, Y. Dauphin, P.S. Liang, and J. Wortman Vaughan (Eds.), Vol. 34. Curran Associates, Inc., Red Hook, NY, USA, 27171–27183.
- Zhou Wang, A.C. Bovik, H.R. Sheikh, and E.P. Simoncelli. 2004. Image quality assessment: from error visibility to structural similarity. *IEEE TIP* 13, 4 (2004), 600–612.
- Zixiong Wang, Yunxiao Zhang, Rui Xu, Fan Zhang, Peng-Shuai Wang, Shuangmin Chen, Shiqing Xin, Wenping Wang, and Changhe Tu. 2023. Neural-Singular-Hessian: Implicit Neural Representation of Unoriented Point Clouds by Enforcing Singular Hessian. *ACM TOG* 42, 6, Article 274 (December 2023), 14 pages. <https://doi.org/10.1145/3618311>
- Tong Wu, Jia-Mu Sun, Yu-Kun Lai, Yuewen Ma, Leif Kobbelt, and Lin Gao. 2024. DeferredGS: Decoupled and Editable Gaussian Splatting with Deferred Shading.
- Ziyi Yang, Yanzhen Chen, Xinyu Gao, Yazhen Yuan, Yu Wu, Xiaowei Zhou, and Xiaogang Jin. 2023. SIRE-IR: Inverse Rendering for BRDF Reconstruction with Shadow and Illumination Removal in High-Illuminance Scenes. arXiv:2310.13030
- Ziyi Yang, Xinyu Gao, Yangtian Sun, Yihua Huang, Xiaoyang Lyu, Wen Zhou, Shaohui Jiao, Xiaojuan Qi, and Xiaogang Jin. 2024. Spec-Gaussian: Anisotropic View-Dependent Appearance for 3D Gaussian Splatting. arXiv:2402.15870
- Lior Yariv, Jiatao Gu, Yoni Kasten, and Yaron Lipman. 2021. Volume Rendering of Neural Implicit Surfaces. In *NeurIPS*, M. Ranzato, A. Beygelzimer, Y. Dauphin, P.S. Liang, and J. Wortman Vaughan (Eds.), Vol. 34. Curran Associates, Inc., Red Hook, NY, USA, 4805–4815.
- Keyang Ye, Qiming Hou, and Kun Zhou. 2024. 3D Gaussian Splatting with Deferred Reflection. In *SIGGRAPH (SIGGRAPH '24)*. Association for Computing Machinery, New York, NY, USA, Article 40, 10 pages. <https://doi.org/10.1145/3641519.3657456>
- Ze-Xin Yin, Jiaxiang Qiu, Ming-Ming Cheng, and Bo Ren. 2023. Multi-Space Neural Radiance Fields. In *CVPR*. IEEE, New York, NY, USA, 12407–12416.
- Mulin Yu, Tao Lu, Linning Xu, Lihan Jiang, Yuanbo Xiangli, and Bo Dai. 2024a. GSDF: 3DGS Meets SDF for Improved Rendering and Reconstruction. arXiv:2311.16473
- Zehao Yu, Torsten Sattler, and Andreas Geiger. 2024b. Gaussian opacity fields: Efficient adaptive surface reconstruction in unbounded scenes. *ACM TOG* 43, 6 (2024), 1–13.
- Jingyang Zhang, Yao Yao, Shiwei Li, Tian Fang, David McKinnon, Yanghai Tsin, and Long Quan. 2022c. Critical Regularizations for Neural Surface Reconstruction in the Wild. In *CVPR*. IEEE, New York, NY, USA, 6270–6279.
- Jingyang Zhang, Yao Yao, Shiwei Li, Jingbo Liu, Tian Fang, David McKinnon, Yanghai Tsin, and Long Quan. 2023. NeLLF++: Inter-Reflectable Light Fields for Geometry and Material Estimation. In *ICCV*. IEEE, New York, NY, USA, 3601–3610.
- Kai Zhang, Fujun Luan, Zhengqi Li, and Noah Snavely. 2022a. IRON: Inverse Rendering by Optimizing Neural SDFs and Materials From Photometric Images. In *CVPR*. IEEE, New York, NY, USA, 5565–5574.
- Kai Zhang, Fujun Luan, Qianqian Wang, Kavita Bala, and Noah Snavely. 2021a. PhysSG: Inverse Rendering With Spherical Gaussians for Physics-Based Material Editing and Relighting. In *CVPR*. IEEE, New York, NY, USA, 5453–5462.
- Richard Zhang, Phillip Isola, Alexei A. Efros, Eli Shechtman, and Oliver Wang. 2018. The Unreasonable Effectiveness of Deep Features as a Perceptual Metric. In *CVPR*. IEEE, New York, NY, USA, 10.
- Xiuming Zhang, Pratul P. Srinivasan, Boyang Deng, Paul Debevec, William T. Freeman, and Jonathan T. Barron. 2021b. NeRFactor: neural factorization of shape and reflectance under an unknown illumination. *ACM TOG* 40, 6, Article 237 (dec 2021), 18 pages.
- Yuanqing Zhang, Jiaming Sun, Xingyi He, Huan Fu, Rongfei Jia, and Xiaowei Zhou. 2022b. Modeling Indirect Illumination for Inverse Rendering. In *CVPR*. IEEE, New York, NY, USA, 18643–18652.

Supplementary Material – GS-ROR²: Bidirectional-guided 3DGS and SDF for Reflective Object Relighting and Reconstruction

1 LOSS DETAILS

We introduce the definition and weights of losses we used in the main paper. The color loss is defined as in 3DGS [Kerbl et al. 2023]

$$L_c = \lambda \|C_{gs} - C_{gt}\|_1 + (1 - \lambda)(1 - \text{SSIM}(C_{gs}, C_{gt})), \quad (1)$$

where C_{gs} is the rendered color from Gaussians and C_{gt} is the ground truth color. The coefficient λ is set to 0.8. The supervision L_{nd} from normal is defined as

$$L_{nd} = \|\hat{\mathbf{n}} - \mathbf{n}\|^2, \quad (2)$$

where $\hat{\mathbf{n}}, \mathbf{n}$ are the normal from depth and the normal from Gaussians, respectively. Our normal formulation follows Gaussian Shader, which combines the shortest axis and a learnable residual [Jiang et al. 2024] as

$$\mathbf{n} = u + n_\delta, \quad (3)$$

where u is the shortest axis and n_δ is the residual term. To prevent the residual from dominating the normal direction, we add a penalty to it:

$$L_{\delta_n} = \|n_\delta\|^2. \quad (4)$$

The smoothness loss for BRDF parameters (*i.e.*, albedo \mathbf{a} , roughness \mathbf{r} , metallicity \mathbf{m}) is defined as

$$L_{sm} = \|\nabla f\| \exp^{-\|\nabla C_{gt}\|}, (f \in \{\mathbf{a}, \mathbf{r}, \mathbf{m}\}) \quad (5)$$

where ∇ is the gradient operator and C_{gt} is the color of ground-truth image. The mask loss is the binary cross entropy between predicted and ground-truth masks.

In the first phase, we set the corresponding weights $\lambda_{[\cdot]}$ as $\lambda_{nd} = 0.2$, $\lambda_{sm} = 1e^{-2}$, $\lambda_m = 0.2$, $\lambda_{\delta_n} = 1e^{-3}$. In the second phase, the loss weights are set as $\lambda_{gs2sdf} = 0.5$, $\lambda_{eik} = 0.1$, $\lambda_{hes} = 5e^{-4}$, $\lambda_{tv} = 0.1$. In third phase, the loss weights are set as $\lambda_{sdf2gs} = 0.25$.

2 SPLIT-SUM APPROXIMATION

A typical rendering equation needs to compute an integral on the upper hemisphere involving incident light, view direction, normal, and BRDF (Bidirectional Reflectance Distribution Function):

$$c(\omega_o) = \int_{\Omega} L_i(\omega_i) f(\omega_i, \omega_o) (\omega_i \cdot \mathbf{n}) d\omega_i, \quad (6)$$

where $L_i(\omega_i)$ denotes the light from incident direction ω_i , $f(\omega_i, \omega_o)$ is the BRDF with respect to the incident direction ω_i and outgoing direction ω_o , and \mathbf{n} denotes the surface normal. In practice, the Disney Principled BRDF [McAuley et al. 2013] is the most widely used BRDF, consisting of a diffuse lobe and a specular lobe

$$f(\omega_i, \omega_o) = \underbrace{(1 - \mathbf{m}) \frac{\mathbf{a}}{\pi}}_{\text{diffuse}} + \underbrace{\frac{DFG}{4(\omega_i \cdot \mathbf{n})(\omega_o \cdot \mathbf{n})}}_{\text{specular}}, \quad (7)$$

where D is the normal distribution function, F is the Fresnel term, G is the geometry term, \mathbf{a} is the albedo, and \mathbf{m} is the metallicity.

Author’s address:

However, the integral is expensive to evaluate, and the split-sum technique [Karis 2013] is an alternative widely used in real-time rendering. The specular term is approximated as

$$c_{\text{specular}} \approx L_{\text{specular}} \cdot ((1 - \mathbf{m}) \times 0.04 + \mathbf{m} \times \mathbf{a}) \times F_1 + F_2, \quad (8)$$

where F_1, F_2 are two scalars from a pre-computed table. The diffuse term is computed as

$$c_{\text{diffuse}} = \frac{\mathbf{a}(1 - \mathbf{m})}{\pi} \cdot L_{\text{diffuse}}. \quad (9)$$

L_{diffuse} and L_{specular} can be directed queried for a pre-filtered environment map or neural light representations. The rendered color $c(\omega_o)$ is computed as $c(\omega_o) = c_{\text{diffuse}} + c_{\text{specular}}$. However, as illustrated in the main paper, with small roughness, the split-sum approximation leads to blurry results.

3 LIGHT MODELING

Considering the efficiency of the light query, we use a simple differential environment map and do not model the indirect illumination and occlusion. The environment light is in the cube map format, whose resolution is $6 \times 512 \times 512$.

4 MORE RESULTS

In this section, we present more results and comparisons.

4.1 Glossy Blender Dataset

We present the LPIPS [Zhang et al. 2018] of relighting images on the Glossy Blender dataset in Tab. 1 and Tab. 2. Our method outperforms Gaussian-based methods along with some NeRF-based ones and is competitive with the current SOTA method. Besides, we present the CD of reconstructed mesh in Tab. 3, our method achieves the second-best average reconstruction quality and beats the TensoSDF. Although our quantitative metrics are lower than NeRO, our training time is much shorter (15% of NeRO). The extra mesh visualization of PGSR is in Fig. 1.

Table 1: Relighting quality with Gaussian-based methods on the Glossy Blender dataset in terms of LPIPS \downarrow .

	GS-IR	R3DG	GShader	Ours
Angel	0.1901	0.1428	0.1181	0.0858
Bell	0.5203	0.1431	0.1329	0.0795
Cat	0.1591	0.1171	0.1114	0.0596
Horse	0.1606	0.0866	0.0498	0.0356
Luyu	0.1391	0.1094	0.1057	0.0672
Potion	0.2142	0.1614	0.1832	0.0937
Tbell	0.3368	0.1970	0.1877	0.0953
Teapot	0.1716	0.1312	0.1194	0.0982
Mean	0.2365	0.1361	0.1260	0.0769

4.2 Shiny Blender dataset

We show the NVS and relighting results on the Shiny Blender dataset [Verbin et al. 2022]. The LPIPS comparison of NVS results is in Tab. 4. We present the relighting result in Fig. 2. Our method provides photo-realistic relighting results, while other Gaussian-based methods fail to render highlights under novel light conditions. We show decomposed maps in Fig. 3, and our method can provide reasonable BRDF decomposition.

Table 2: Relighting quality with NeRF-based methods on the Glossy Blender dataset in terms of LPIPS \downarrow .

	TensoIR	MII	TensoSDF	NeRO	Ours
Angel	0.2739	0.1404	0.0871	0.1923	0.0858
Bell	0.2806	0.1534	0.0263	0.0189	0.0795
Cat	0.2146	0.1429	0.0675	0.0455	0.0596
Horse	0.2913	0.0713	0.0318	0.0410	0.0356
Luyu	0.2463	0.1393	0.0807	0.0696	0.0672
Potion	0.2954	0.1747	0.0759	0.0623	0.0937
Tbell	0.2786	0.1938	0.0543	0.0407	0.0953
Teapot	0.2030	0.1426	0.0485	0.0193	0.0982
Mean	0.2605	0.1448	0.0590	0.0612	0.0769

Table 3: Mesh quality in terms of CD \downarrow on the Glossy Blender dataset. (CD is multiplied by 10^2) Numbers in red indicate the best performance, and numbers in orange indicate the second best. Our method outperforms most existing NeRF-based methods. Note that although our quantitative metrics are lower than NeRO, our training time is much shorter (15% of NeRO).

	MII	TensoIR	TensoSDF	NeRO	Ours
Angel	0.77	29.84	0.63	0.34	0.41
Bell	0.69	34.75	0.72	0.32	0.31
Cat	1.14	24.45	1.68	0.43	1.34
Horse	0.55	33.67	0.37	0.44	0.34
Luyu	0.90	22.46	0.63	0.53	0.81
Potion	0.78	19.60	0.61	0.51	0.75
Tbell	0.67	24.38	0.50	0.34	0.55
Teapot	0.74	27.70	0.73	0.33	0.47
Mean	0.78	27.11	0.73	0.41	0.62

Table 4: NVS quality with Gaussian-based methods on Shiny Blender dataset in terms of LPIPS \downarrow .

	GS-IR	R3DG	GShader	Ours
Ball	0.2966	0.2169	0.1358	0.0842
Car	0.0849	0.0533	0.0477	0.0330
Coffee	0.1125	0.0841	0.0853	0.1035
Helmet	0.1618	0.1014	0.0866	0.0482
Teapot	0.0222	0.0097	0.0108	0.0079
Toaster	0.2479	0.1523	0.1017	0.0859
Mean	0.1543	0.1030	0.0779	0.0605



Figure 1: Additional mesh comparison with PGSR [Chen et al. 2024].

4.3 TensoIR synthetic dataset

We present the relighting quality of Gaussian-based methods on the TensoIR synthetic dataset [Jin et al. 2023] in terms of LPIPS in Tab. 5 and the relighting visualization in Fig. 4. The relighting comparison with NeRF-based methods is in terms of PSNR, SSIM in Tab. 6 and LPIPS in Tab. 7. And the relighting visualization of NeRF-based methods is in Fig. 5. We also show the decomposed maps in Fig. 6, and the comparison of normal with Gaussian-based methods in Fig. 7. These results of diffuse objects reveal that though our design focuses on reflective surfaces, it can benefit diffuse objects.

Table 5: Relighting quality with Gaussian-based methods on the TensoIR synthetic dataset in terms of LPIPS \downarrow .

	GS-IR	R3DG	GShader	Ours
Armada.	0.0821	0.0593	0.0649	0.0482
Ficus	0.0956	0.0366	0.0437	0.0439
Hotdog	0.1408	0.0880	0.1275	0.0771
Lego	0.1193	0.0902	0.1423	0.0724
Mean	0.1095	0.0685	0.0946	0.0604

Table 6: Relighting quality with NeRF-based methods on the TensorIR synthetic dataset in terms of PSNR \uparrow and SSIM \uparrow .

	MII	NeRO	TensoSDF	TensorIR	Ours
Armad.	26.85/.9441	23.02/.9335	23.02/.9355	34.51/.9754	31.33/.9593
Ficus	20.65/.9068	27.43/.9404	28.53/.9499	24.32/.9465	26.28/.9542
Hotdog	22.65/.9011	20.45/.9262	20.47/.9241	27.92/.9324	25.21/.9307
Lego	23.20/.8643	17.76/.8577	17.92/.8670	27.61/.9253	25.46/.9083
Mean	23.34/.9041	22.17/.9145	22.48/.9191	28.59/.9449	27.07/.9381

Table 7: Relighting quality with NeRF-based methods on the TensorIR synthetic dataset in terms of LPIPS \downarrow .

	MII	NeRO	TensoSDF	TensorIR	Ours
Armad.	0.0692	0.0644	0.0578	0.0368	0.0483
Ficus	0.0728	0.0677	0.0533	0.0543	0.0439
Hotdog	0.0893	0.0888	0.0906	0.0833	0.0771
Lego	0.1715	0.1228	0.1088	0.0702	0.0723
Mean	0.1007	0.0859	0.0776	0.0612	0.0604

REFERENCES

- Danpeng Chen, Hai Li, Weicai Ye, Yifan Wang, Weijian Xie, Shangjin Zhai, Nan Wang, Haomin Liu, Hujun Bao, and Guofeng Zhang. 2024. PGSR: Planar-based gaussian splatting for efficient and high-fidelity surface reconstruction. *IEEE TVCG* (2024).
- Yingwenqi Jiang, Jiadong Tu, Yuan Liu, Xifeng Gao, Xiaoxiao Long, Wenping Wang, and Yuexin Ma. 2024. GaussianShader: 3D Gaussian Splatting with Shading Functions for Reflective Surfaces. In *CVPR*. IEEE, New York, NY, USA, 5322–5332.
- Haian Jin, Isabella Liu, Peijia Xu, Xiaoshuai Zhang, Songfang Han, Sai Bi, Xiaowei Zhou, Zexiang Xu, and Hao Su. 2023. TensorIR: Tensorial Inverse Rendering. In *CVPR*. IEEE, New York, NY, USA, 165–174.
- Brian Karis. 2013. Real shading in unreal engine 4. *Proc. Physically Based Shading Theory Practice* (2013).
- Bernhard Kerbl, Georgios Kopanas, Thomas Leimkühler, and George Drettakis. 2023. 3D Gaussian Splatting for Real-Time Radiance Field Rendering. *ACM TOG* 42, 4 (2023), 139–1.
- Stephen McAuley, Stephen Hill, Adam Martinez, Ryusuke Villemin, Matt Pettineo, Dimitar Lazarov, David Neubelt, Brian Karis, Christophe Hery, Naty Hoffman, and Hakan Zap Andersson. 2013. Physically based shading in theory and practice. In *ACM SIGGRAPH 2013 Courses (SIGGRAPH '13)*. Association for Computing Machinery, New York, NY, USA, Article 22, 8 pages. <https://doi.org/10.1145/2504435.2504457>
- Dor Verbin, Peter Hedman, Ben Mildenhall, Todd Zickler, Jonathan T. Barron, and Pratul P. Srinivasan. 2022. Ref-NeRF: Structured View-Dependent Appearance for Neural Radiance Fields. In *CVPR*. IEEE, New York, NY, USA, 5491–5500.
- Richard Zhang, Phillip Isola, Alexei A. Efros, Eli Shechtman, and Oliver Wang. 2018. The Unreasonable Effectiveness of Deep Features as a Perceptual Metric. In *CVPR*. IEEE, New York, NY, USA, 10.

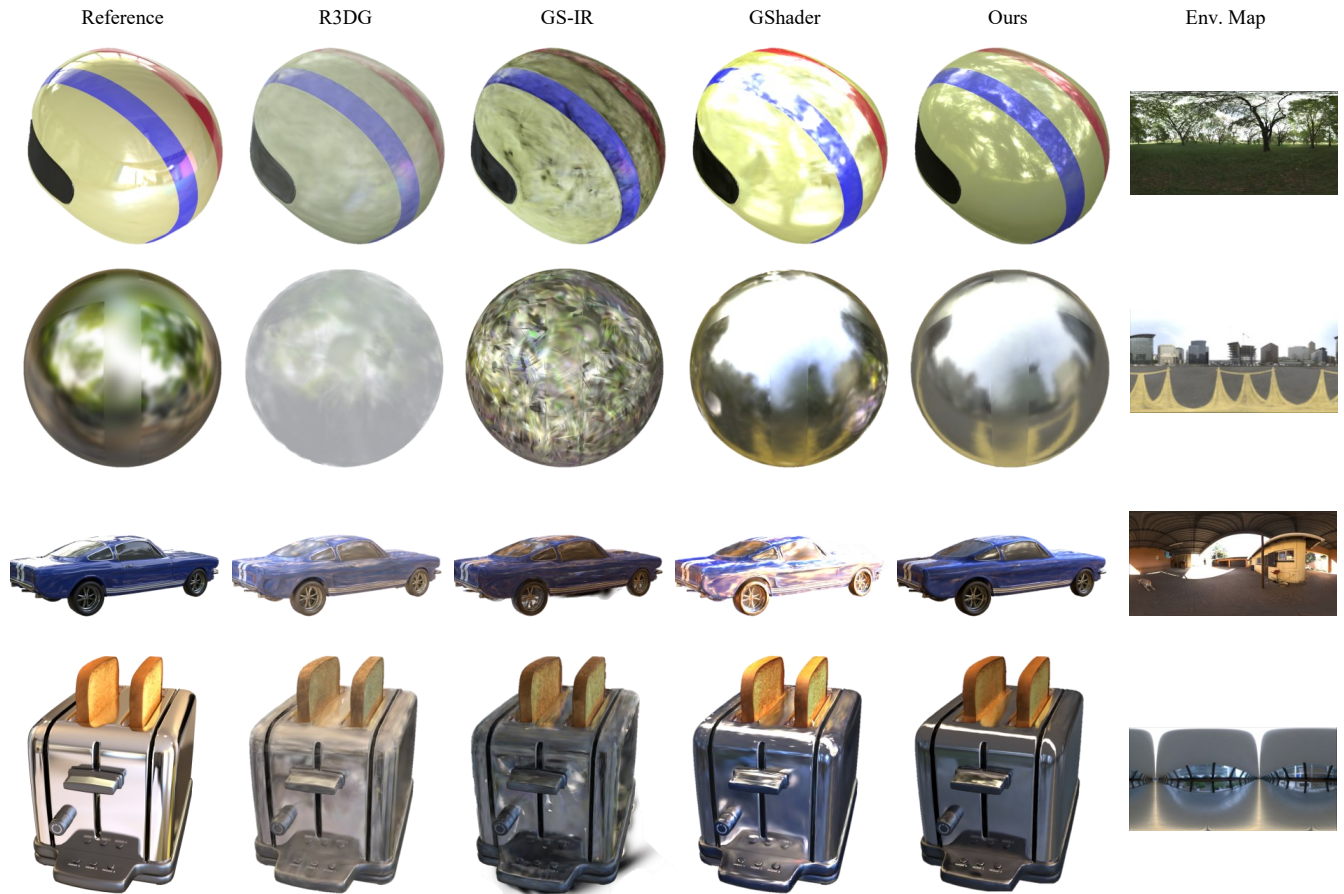


Figure 2: Relighting results of Gaussian-based methods on the Shiny Blender dataset. Note that no relighting ground truth is available, so we only show the relighting examples. Our method can provide reasonable relighting results under diverse lighting conditions.

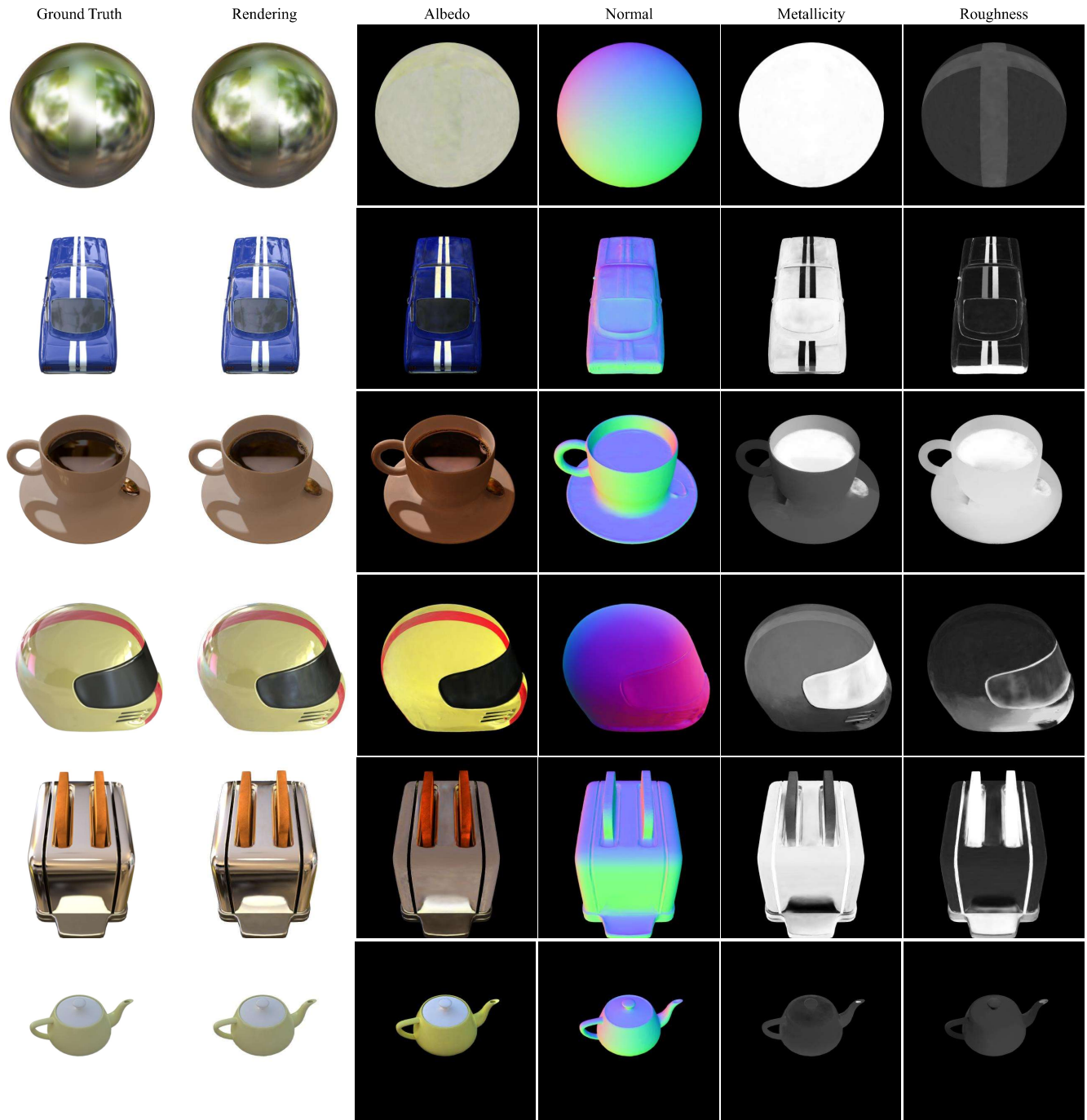


Figure 3: Normal and BRDF decomposed maps on the Shiny Blender dataset. Our method provides robust normal estimation and reasonable BRDF decomposition.



Figure 4: Relighting results of Gaussian-based methods on the TensoIR synthetic dataset. Our method can also provide high-quality relighting results for diffuse objects and outperforms the existing Gaussian-based methods.



Figure 5: Relighting results of NeRF-based methods on the TensoIR synthetic dataset. Our method can also provide high-quality relighting results for diffuse objects and outperforms most NeRF-based methods.

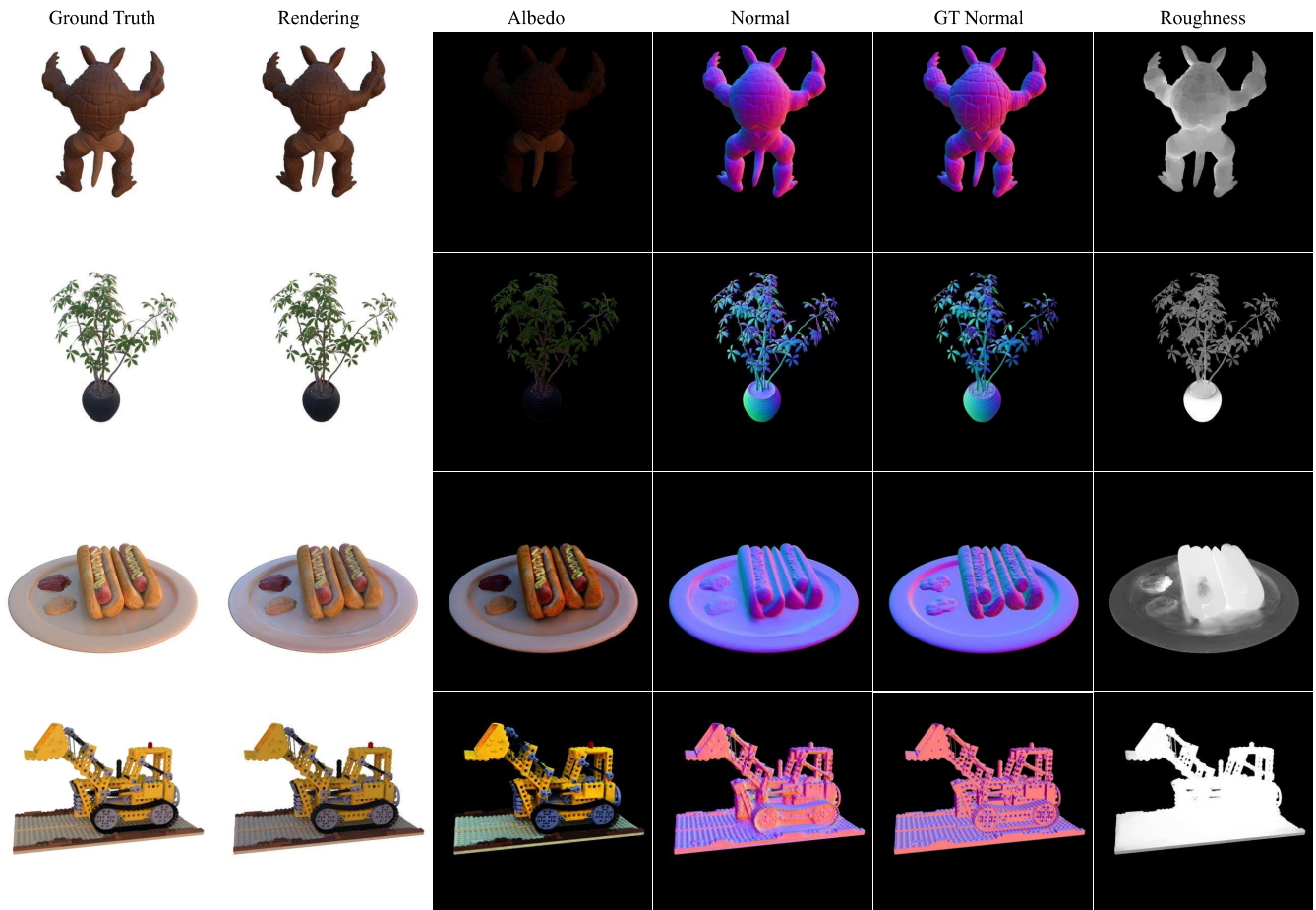


Figure 6: Normal and BRDF decomposed maps of our method on the TensoIR synthetic dataset. Our method can also provide reasonable BRDF estimation for diffuse objects.

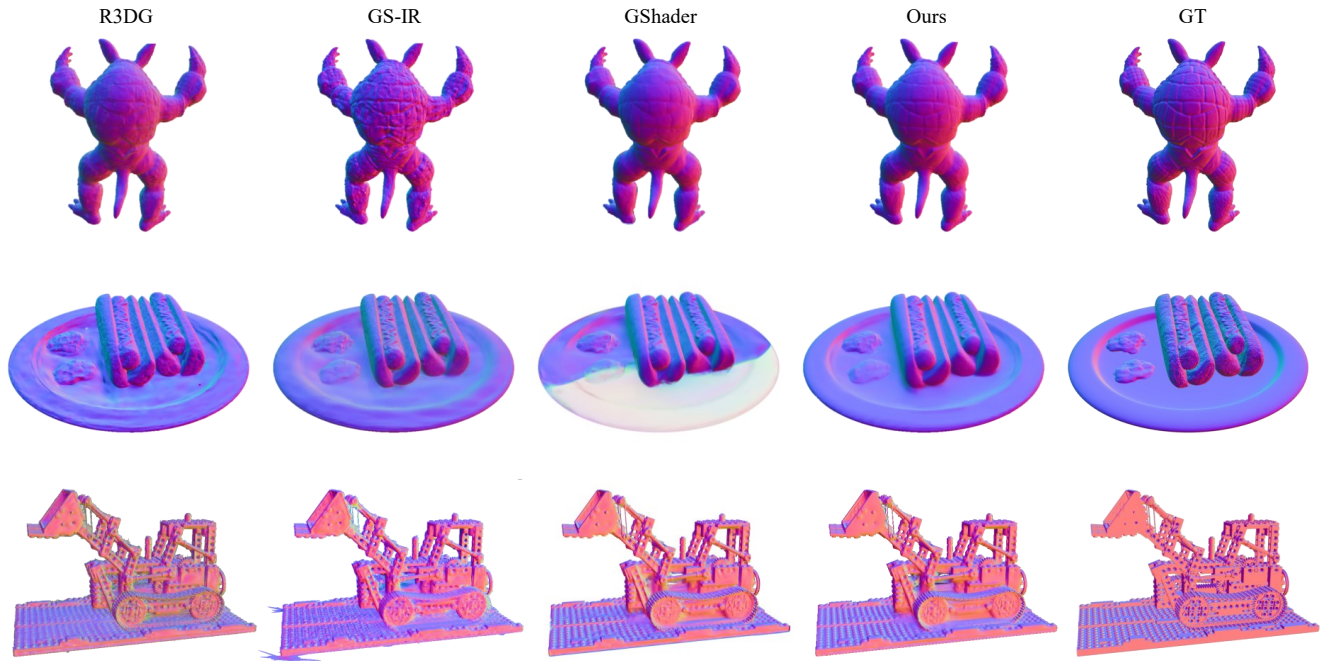


Figure 7: Normal comparison with Gaussian-based methods on the TensoIR synthetic dataset. Our method can also provide robust normal estimation for diffuse objects.

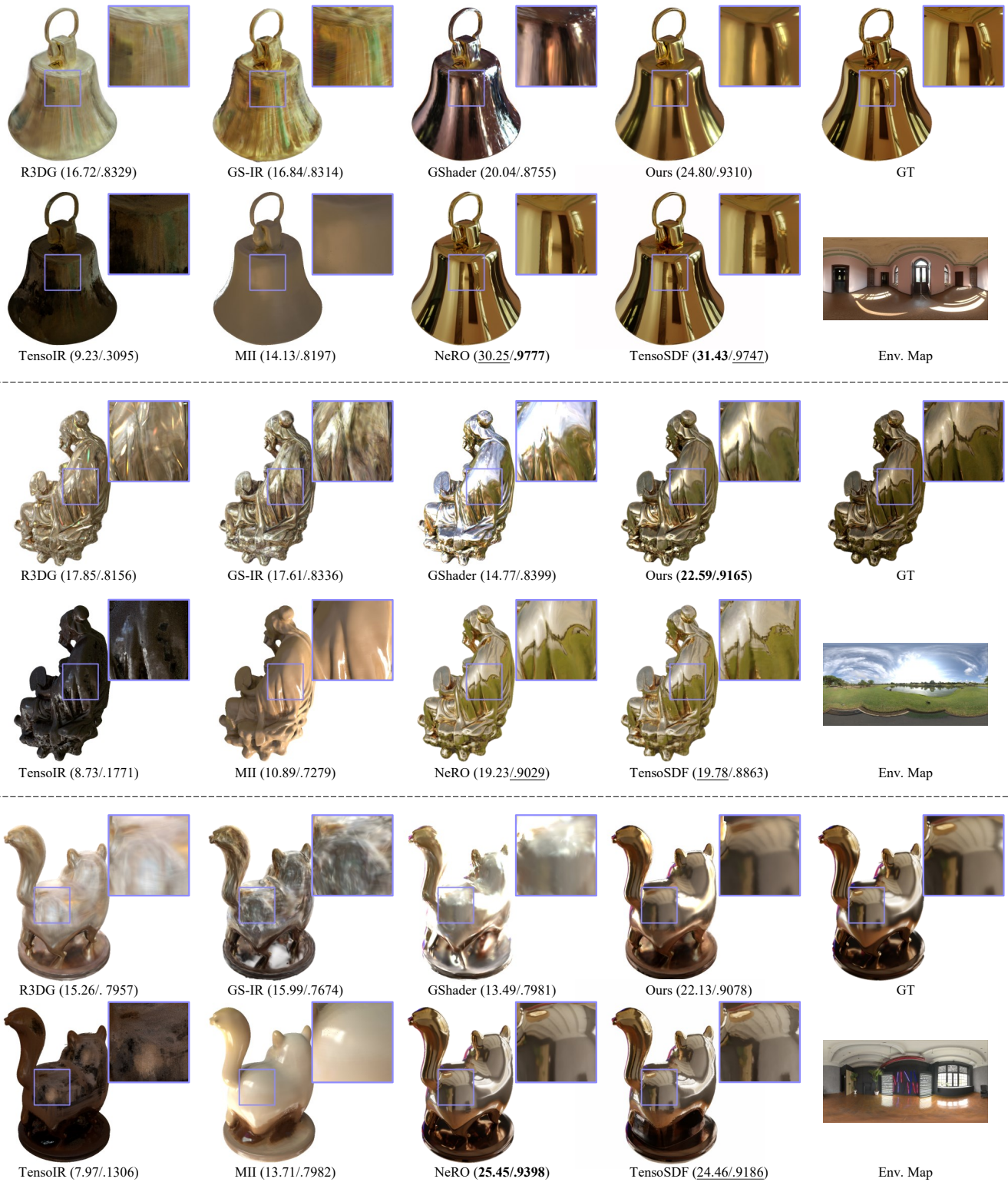


Fig. 14. Relighting results on the Glossy Blender Dataset. R3DG, GS-IR, TensoIR, and MII fail to model specular highlights. GShader provides specular relighting results with obvious artifacts. Our method, along with NeRO and TensoSDF, provides high-quality results, while our method only uses 25% training time of TensoSDF and enables real-time relighting. We present the metrics per scene (PSNR/SSIM).

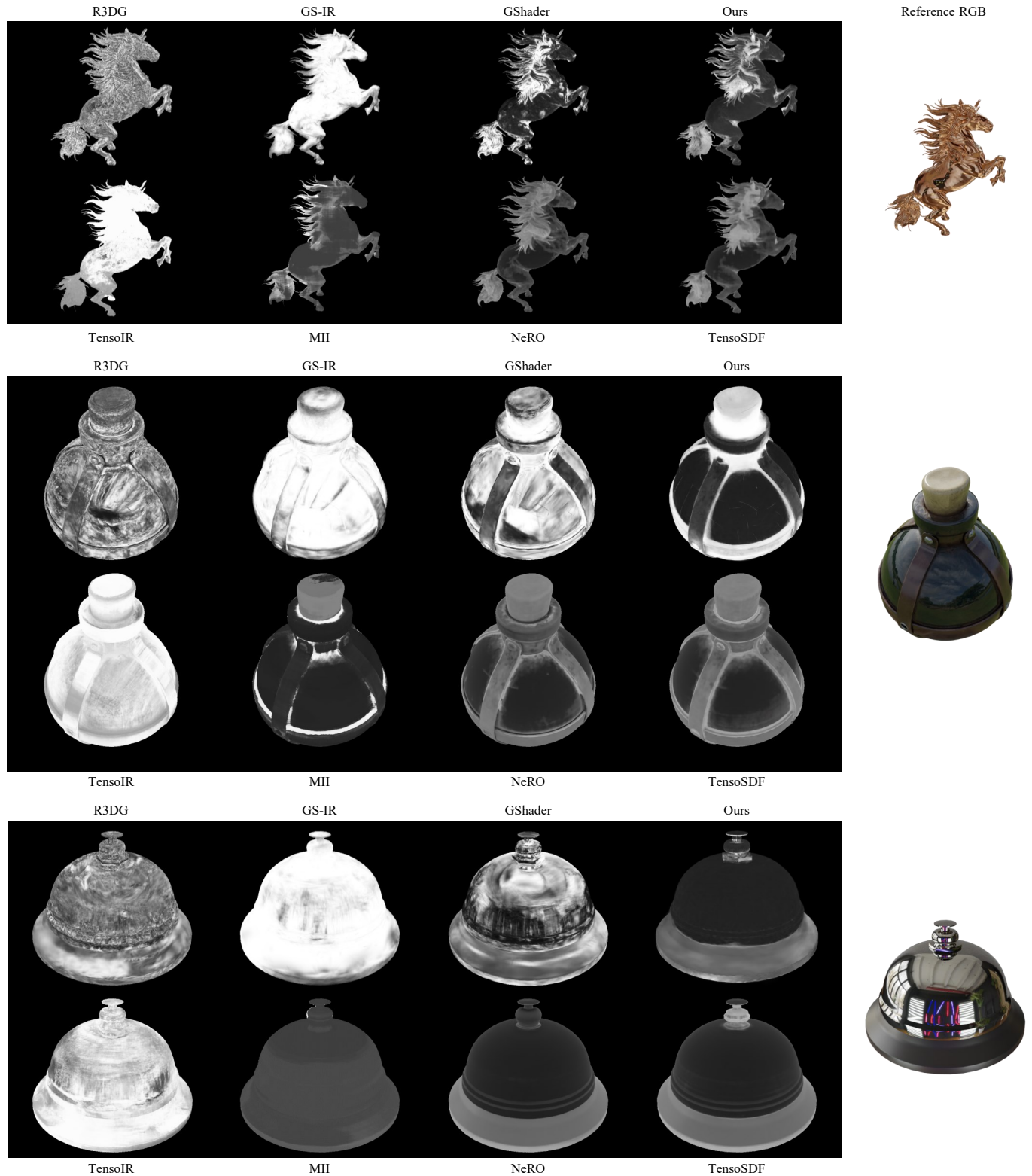


Fig. 15. Decomposed roughness visualization on the Glossy Blender Dataset. Gaussian-based methods and TensoIR reconstruct problematic roughness. MII provides over-smooth prediction and ignores the difference of material. Our method, NeRO, and TensoSDF reconstruct reasonable roughness for relighting, while our method takes 25% training time at most.

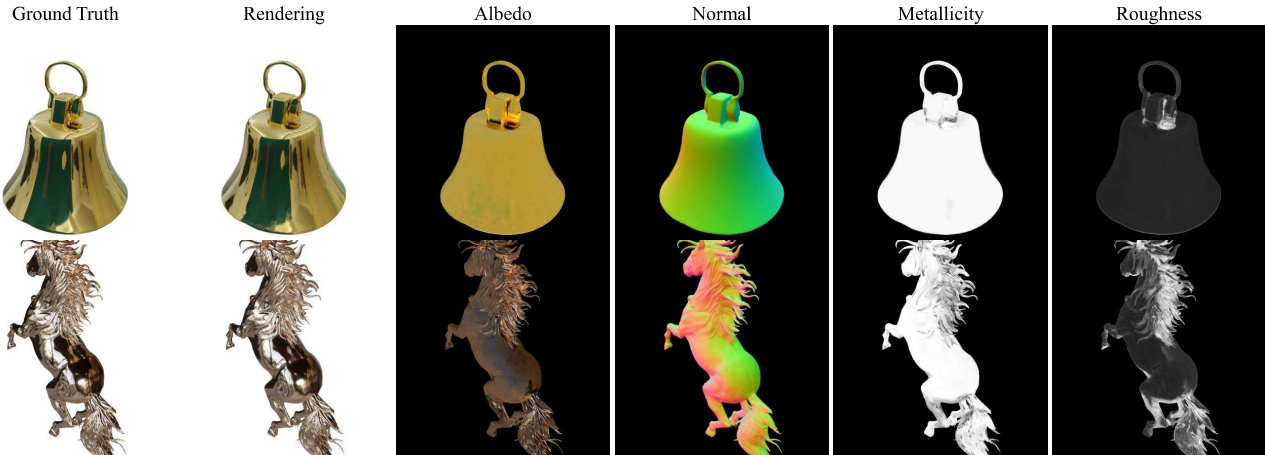


Fig. 16. Decomposed maps of our method on the Glossy Blender Dataset. Our method can provide a reasonable decomposition for reflective surfaces. The normal is smooth but maintains details (see the horse mane in the 2nd row). There is no material ground truth, so we only provide the qualitative visualization.

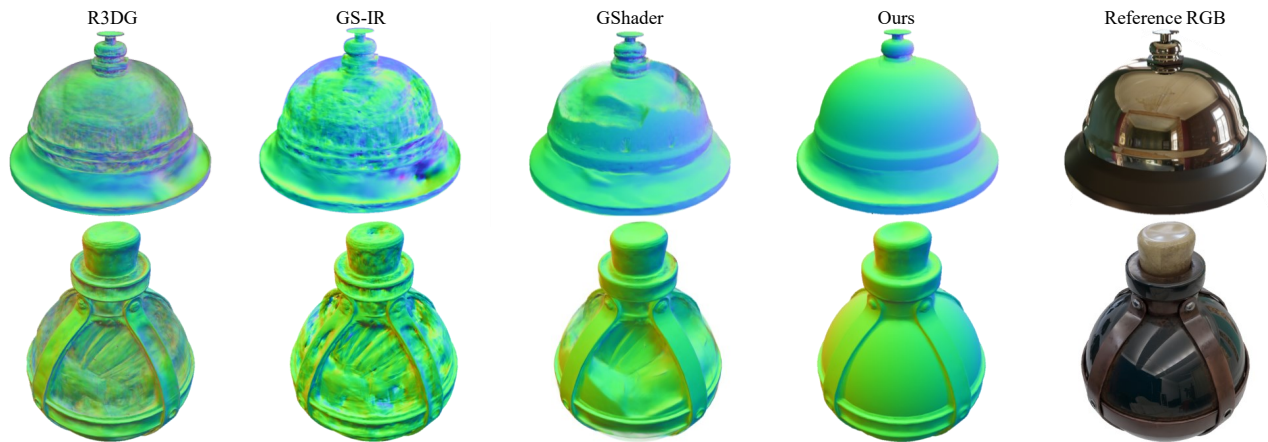


Fig. 17. Normal comparison among Gaussian-based methods on the Glossy Blender Dataset. Our method can reconstruct high-quality normal for relighting, while others overfit under the training scene and provide erroneous normal.

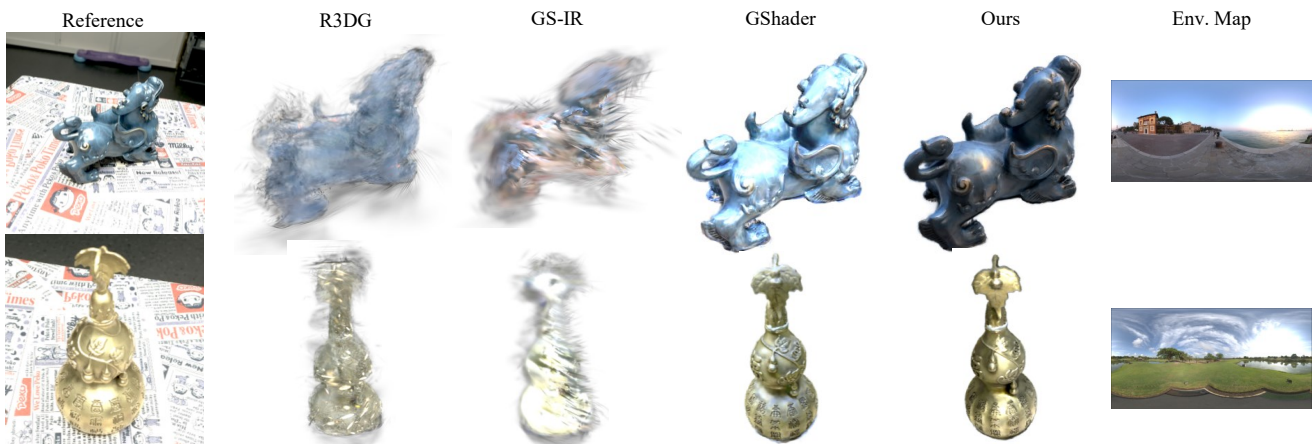


Fig. 18. Relighting results on real data from NeLF++. R3DG and GS-IR fail to reconstruct the reflective objects in real scenes. GShader cannot relight the specular highlights faithfully, while our method can provide reasonable relighting results.



Fig. 19. NVS results on the Glossy dataset. Our method provides photo-realistic NVS results for reflective objects, while other Gaussian-based methods fail.

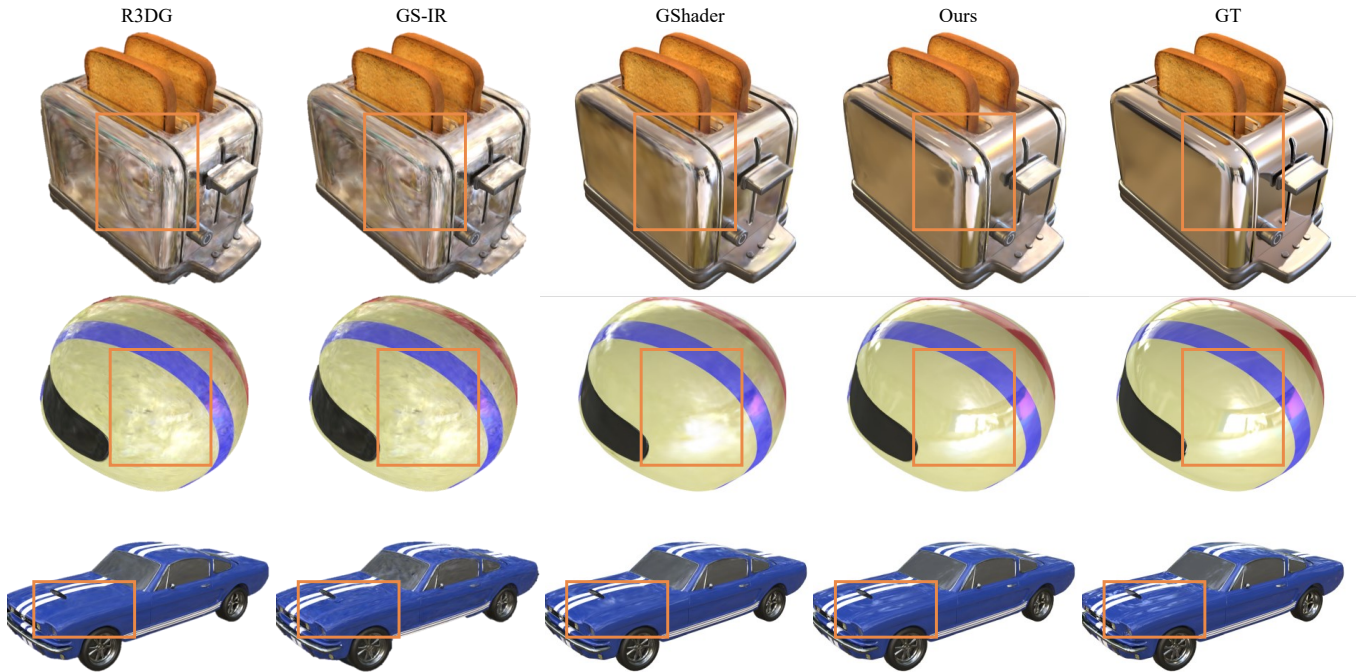


Fig. 20. NVS results of Gaussian-based methods on the Shiny Blender dataset. Our method preserves correct highlights, while others fail to render sharp highlights.

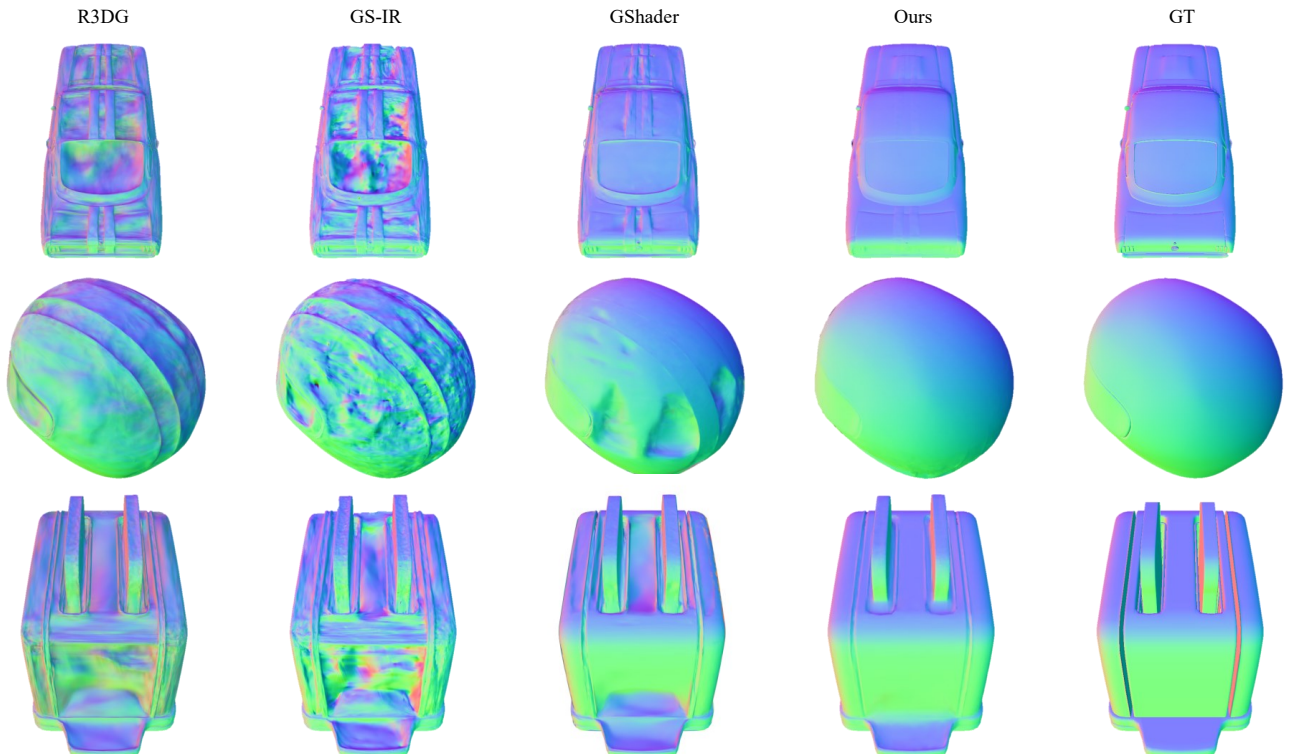


Fig. 21. Normal comparison with Gaussian-based methods on the Shiny Blender dataset. Our method provides robust normal estimation, while other results are noisy or overfitted.



Fig. 22. Mesh comparison on the Glossy Blender dataset. Our method provides high-quality meshes from the finetuned TensoSDF. All Gaussian-based methods fail to reconstruct smooth surfaces for reflective objects, while NeRF-based methods cannot preserve the geometry details. Our method ensures both global smoothness and local details. Note that the ground-truth meshes of this dataset are unavailable (only point cloud is available), so we choose to show the RGB reference under the nearest viewpoint on the dataset. Due to the limited space, we present the PGSR results in the supplementary.